https://doi.org/10.5194/egusphere-2026-3619
Preprint. Discussion started: 26 June 2026


# The impact of the Hunga eruption on the 2023 Antarctic ozone hole: contrasting effects in the core and edge regions of the polar vortex

Saffron G. Heddell[1], Martyn P. Chipperfield[1,2], Graham W. Mann[1,3], Sandip S. Dhomse[1,2,3], Wuhu Feng[1,3], Xin Zhou[4], Masaru Yoshioka[1], and Anthony Jones[5]

[1]School of Earth, Environment, and Sustainability, University of Leeds, Leeds, United Kingdom
[2]National Centre for Earth Observation, University of Leeds, Leeds, UK
[3]National Centre for Atmospheric Science, University of Leeds, Leeds, UK
[4]School of Atmospheric Sciences, Chengdu University of Information Technology, Chengdu, China
[5]Met Office, Exeter, UK

**Correspondence:** Saffron G. Heddell (eesgh@leeds.ac.uk)

**Abstract.** The January 2022 Hunga eruption injected an exceptional 150 Tg of water vapour ($H_2O$) into the stratosphere causing an enhancement not observed previously within the satellite era, with extensive and ongoing effects. From global chemical transport model simulations, we further assess the high-latitude $H_2O$ enhancement caused by the eruption, and how it influenced the 2023 Antarctic ozone depletion across two vortex regimes: the cold core and the less cold, and more insolated vortex edge region. Our simulations show the $H_2O$ chemical impacts arose mainly from the $H_2O$ enhancement promoting earlier formation of polar stratospheric clouds (PSCs), which in turn enhanced chlorine activation and subsequent ozone loss. We also show ice PSC dehydration in the vortex core limited Hunga's chemical effects to occur for only the first 25% of the vortex season; consequently, the edge region experienced the largest chemical impact to ozone depletion in 2023. Overall, the $H_2O$ enhancement increased Antarctic ozone hole area by 7% but remaining within the historical variability over the past two decades. Sensitivity simulations including the Hunga sulfate aerosol show $H_2O$-driven heterogeneous chlorine activation on additional PSCs, dominated the chemical impacts of Hunga on polar ozone, with only minor impact from activation on volcanic sulfate aerosol. Our results highlight that while water-rich large volcanic eruptions can worsen polar ozone depletion, the magnitude of the impact is strongly influenced by stratospheric temperatures through dehydration. This suggests that less cold vortex environments, e.g. the Arctic, may experience larger relative changes in chlorine activation under similar conditions.

## 1 Introduction

### 1.1 The eruption

The Hunga submarine volcano (20.54°S, 175.38°W) entered an explosive phase on December 20$^{th}$, 2021 culminating in a series of climactic explosions on 15th January 2022. This eruption was comparable in explosive energy to Krakatoa in August 1883 (Wright et al., 2022), reaching a volcanic explosivity index (VEI) 6 (Poli and Shapiro, 2022; Newhall and Self, 1982). The eruption produced several notable volcanic hazards, including the record of the highest eruption plume observed in the satellite era with the overshooting top reaching altitudes of up to 58 km (Proud et al., 2022), thereby breaching into the mesosphere.

https://doi.org/10.5194/egusphere-2026-3619
Preprint. Discussion started: 26 June 2026


Hunga emitted 150 Tg of water vapour ($H_2O$) into the stratosphere (e.g. Millán et al., 2022), increasing the global stratospheric $H_2O$ burden by approximately 10%. The stratospheric injection of $SO_2$ was estimated to be 0.4 - 0.5 Tg (e.g. Carn et al., 2022), later revised to 0.4 - 1 Tg by some studies (e.g. Carn, Schmidt, et al., 2025).

The Hunga $H_2O$ was transported throughout the stratosphere by the Brewer-Dobson circulation (BDC), initially confined to the southern hemisphere due to the location of the eruption. Both observations and modelling show that the $H_2O$ did not reach the Antarctic until June/July 2022, by which time that year's Antarctic vortex had formed (e.g., Manney et al., 2023; Zhou et al., 2024; Wang, Coy et al., 2025). The vortex boundary then acted as a barrier (e.g. Roscoe et al., 2012) and the $H_2O$ was not able to penetrate into the highest latitudes until November 2022, following the vortex break up (e.g. Manney et al., 2023). Therefore, in this study we focus on April-December 2023 which was the first Antarctic vortex season to be chemically perturbed by the Hunga $H_2O$ enhancement. Both observations and early model results have shown that the Hunga $H_2O$ enhancement led to an increase in ozone depletion in the 2023 Antarctic spring, once the $H_2O$ reached high latitudes (e.g. Manney et al., 2023; Wohltmann et al., 2024; Zhou et al., 2024; Fleming et al., 2024). The Hunga eruption has been further studied using space- and ground-based observations and numerical models in a recently completed major report (APARC, 2025), including the intermodel, and model-to-measurement comparisons - Hunga Tonga–Hunga Ha'apai Model Observations Comparison (HTHH-MOC) (Zhu et al., 2024) and Hunga Tonga–Hunga Ha'apai Volcano Model Intercomparison Project (Tonga-MIP) (Clyne et al., 2024).

The ozone impacts chapter of the APARC Hunga report (Østerstrøm, Santee, et al., 2025) establishes that the Hunga eruption did cause some additional ozone depletion within the 2023 Antarctic vortex but was unexceptional within the context of the interannual variability. However, the spread of the impact estimated from models is relatively large, which is thought to be, at least in part, due to the varied definitions of the vortex area. Although the Antarctic vortex can be considered relatively stable in comparison to its Arctic counterpart, it is still mobile especially at the beginning and end of the season. Therefore, the studies that use a static definition such as the polar cap (60°S–90°S) are likely to be incorporating outside vortex air or missing portions of the edge in their analysis. Whilst the APARC report and related studies (e.g. Zhou et al., 2024; Santee et al., 2024) do highlight the maximum increased ozone depletion as occurring within the Antarctic vortex edge and identify possible explanations related to the saturation of the chemical processing, they do not explicitly separate the vortex core and edge regions. This study therefore extends the analysis of the Hunga eruption on the 2023 Antarctic vortex considering the chemical and environmental differences between the vortex regions using a vortex-following regime to define the regions and ensure that air masses are correctly categorised. For the analysis in this study, we use a 3-D global chemical transport model to focus on the chemical impact of the eruption on the stratospheric ozone rather than dynamical impacts.

### 1.2 Volcanoes and the stratosphere

Impacts from previous stratospheric reaching eruptions, such as El Chichon (1982) and Mount Pinatubo (1991) (e.g. Dhomse et al., 2020; Wang et al., 2023) have generally stemmed from their sulphate aerosol injections (e.g. Wilmouth et al., 2023). Stratospheric sulfate aerosol (SSA) due to volcanic eruptions is a significant contributing factor to natural climate variability and stratospheric dynamics by cooling the surface and warming the stratosphere through the absorption of terrestrial long-wave

https://doi.org/10.5194/egusphere-2026-3619
Preprint. Discussion started: 26 June 2026


radiation and near-infrared solar radiation (e.g. Kremser et al., 2016). Volcanic SSA has been known to chemically increase ozone depletion, increasing the ozone hole size as a result, by acting as surfaces for heterogeneous reactions. This can also impact stratospheric dynamics and temperatures through reducing the ultraviolet absorption by ozone (e.g. Robock, 2000). Volcanic SSA tends to stay in the stratosphere for a relatively short duration, on the order of 1 to 3 years (Dyer, 1974; Toohey et al., 2011, 2025), with the longevity of their effects generally on that time scale (Hofmann and Solomon, 1989; Thomason et al., 1997; Dhomse et al., 2015). In contrast, the Hunga $H_2O$ enhancement is projected to take 7 years to decay back to background variability, remaining in the stratosphere until ∼2030 (Zhou et al., 2026). This difference in timescales between the aerosol and $H_2O$ is in part due to the removal mechanisms. The aerosol particles are susceptible to gravitational settling, whereas the removal mechanism of the largely gas-phase $H_2O$ is much more dependent on the stratospheric circulation, descent at the poles (Joshi and Jones, 2009; Vömel et al., 2022), and dehydration via PSCs within the polar vortices (Zhou et al., 2024) consistent with the typical stratospheric circulation timescale of 5-10 years (Hall and Waugh, 1997). A significant challenge for research into the stratospheric impacts of volcanic eruptions is the rarity of large-scale explosive eruptions, and the dependence on the location. Therefore, unprecedented eruptions such as Hunga provide important opportunities to improve our knowledge about their impact on the atmosphere and climate system.

### 1.3 Polar stratospheric clouds and ozone depletion

Metrics for the size of each year's Antarctic ozone hole have shown an overall decreasing trend over the past couple of decades following the implementation of policies under the Montreal Protocol (World Meteorological Organization (WMO)., 2022). However, the Antarctic ozone holes between 2020 and 2023 have been anomalously large, including impacts from the 2019/2020 Australian new year wildfires (e.g. Damany-Pearce et al., 2022; Solomon et al., 2023; Wargan et al., 2025). Polar stratospheric clouds (PSCs) are a crucial component, alongside cold temperatures and sunlight, contributing to the significant ozone depletion in the Antarctic stratosphere and the formation of the ozone hole. PSC particles provide surfaces for heterogeneous reactions that convert the relatively inert reservoir chlorine species into the active chlorine species, as well as removing the nitric acid ($HNO_3$) (denitrification) or $H_2O$ (dehydration) from the system through gravitational sedimentation of the particles (Tritscher et al., 2021). The active species produced from the heterogeneous reactions then catalyse ozone depletion in the springtime when sunlight returns, which begins earlier in the edge region than the core (e.g. Roscoe et al., 2012).

PSCs form only at very low temperatures (below ∼195 K), such conditions occurring extensively within the Antarctic stratospheric vortex each winter polar night. The temperatures at which PSC form depend also on ambient concentrations of gas phase nitric acid and water vapour (Hanson and Mauersberger, 1988), with solid NAT and liquid ternary PSCs both forming from stratospheric sulphate aerosol, respectively by crystallization (James et al., 2018, 2023) and uptake of nitric acid and extra water vapour (Carslaw et al., 1995). Broadly speaking there are three main types of PSC particle - nitric acid trihydrate (NAT), supercooled ternary solution (STS), and ice, historically known as type Ia, Ib, and II (Tritscher et al., 2021). Ice and NAT particles both solid particles composed of $H_2O$ and a mixture of $HNO_3 \cdot 3H_2O$ respectively (e.g. Toon et al., 1986; Crutzen and Arnoldt, 1986), and STS are liquid particles composed of $H_2SO_4$, $HNO_3$, and $H_2O$ (e.g. Molina et al., 1993; Carslaw et al.,

https://doi.org/10.5194/egusphere-2026-3619
Preprint. Discussion started: 26 June 2026


1995). The solid PSCs are responsible for the denitrification and dehydration when the particles reach a large enough size to sediment (Tritscher et al., 2021). All three PSC types are important for explaining the ozone depletion that leads to the ozone hole and form at different threshold temperatures. As temperatures reduce through an Antarctic winter, colder temperatures are required to form liquid STS (around 192 K, e.g. Carslaw et al. (1995)), than for NAT particles, which form at around 195 K (Toon et al., 1986), for typical lower stratospheric conditions, ice PSCs only forming around 188 K (Alfred et al., 2007).

Stratospheric $H_2O$ plays key role in the formation and behaviour of PSCs (Tritscher et al., 2021), therefore increases from events such as Hunga, can lead to changes that will impact the associated heterogeneous reactions, dehydration, and denitrification (e.g Wohltmann et al., 2024). An increase of $H_2O$ equivalent to $\sim$1 ppm has been linked to increases of the PSC formation temperatures (Khosrawi et al., 2016); the increase for ice particles is $\sim$1.1 K (Marti and Mauersberger, 1993) and for NAT it is $\sim$0.8 K (Hanson and Mauersberger, 1988). The STS PSCs are slightly more complicated as there is no sharp threshold temperature but a good estimation based on their reactivity is approximately 1 K increase per 1 ppm $H_2O$ increase (Carslaw et al., 1995). These impacts are only possible before dehydration sets in. Increases in $H_2O$ may also increase particle size which will impact dehydration and denitrification through particle sedimentation rates. In this study, we only address the areal extent of the ice and NAT PSCs, and not explicitly the particle sizes. Hunga provides a useful natural testcase for this hypothesis that increased $H_2O$ due to climate change will increase the temperature at which the PSCs can form and therefore increase their areal extent (e.g. von der Gaathen et al., 2021).

Here we investigate the impact of the January 15, 2022, Hunga eruption on Antarctic chemical ozone depletion during the 2023 season (April to December) using a series of global 3-D chemical transport model simulations mainly focussing on isolating the impacts from the $H_2O$ enhancement. We expand on previous publications by explicitly separating the Antarctic vortex core and edge regions. By doing so, we aim to quantify regional differences in the Hunga-related chemical impacts from the Hunga water-vapour enhancement, and briefly the volcanic sulfate aerosol. We also compare and discuss the main driving or limiting factors for the different responses in the ozone chemistry in the two regions.

This paper is structured as follows. Section 2 provides the details of the methods and the rationale for the vortex region separation (2.1.1), PSC reactions (2.2.1) and areal extents (2.2.2). Section 3 briefly describes the TOMCAT chemical transport model, the simulations and experiments, and summarises the observations used to support the model results. Section 4 presents the results and discussion of the impacts of the Hunga $H_2O$ enhancement on the processes leading to the ozone depletion. Section 5 discusses our results into the context of the ozone hole and isolates the contribution of the enhanced sulfate aerosol to the chemical impact on the ozone chemistry. Section 6 summarises our results focussing on the differences and similarities between the two regions and the mechanisms driving them.

## 2 Metrics to assess chemical perturbations to Antarctic ozone

### 2.1 Introduction to the core and edge regions of the Antarctic vortex

It is recognised that polar ozone chemistry should be analysed by separating the vortex into two distinct regions, the core and edge, due to their differences in temperature, PSC occurrence, and photochemical conditions (e.g. Lee et al., 2001). Both

https://doi.org/10.5194/egusphere-2026-3619
Preprint. Discussion started: 26 June 2026


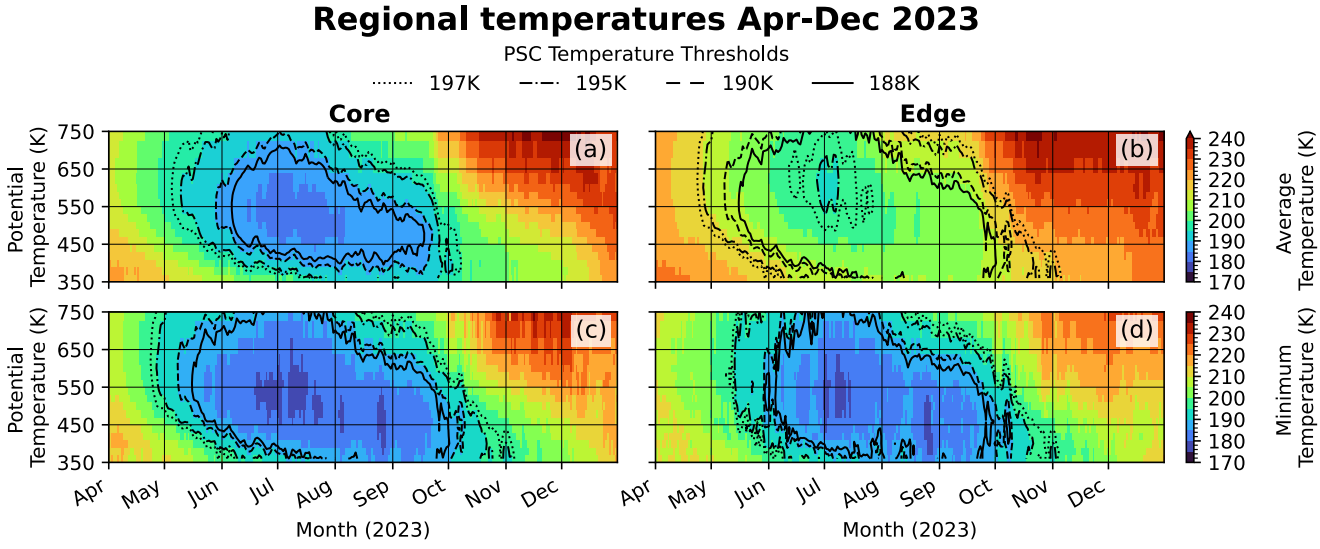


**Figure 1.** Average (a, b) and minimum (c, d) temperatures (K) for the core (a,c) and edge (b, d) regions for April to December 2023 from the ECMWF ERA 5 reanalysis used to force the 3-D CTM. The 195 K, NAT PSC (red) and 188 K, ice PSC (black) temperature thresholds are marked as solid contour lines with the thresholds +2 K as dashed lines. For both rows the left panel is for the core region ($-90°$ to $-70°$ equivalent latitude (EL)) and right is the edge ($-70°$ to $-55°$ EL).

regions show significant differences in timing of chlorine activation, dehydration, and denitrification which can all be perturbed by volcanic eruptions. Figure 1 uses the European Centre for Medium-Range Weather Forecasts (ECMWF) ERA5 temperatures (Hersbach et al., 2020) to illustrate the differences in the vortex-average (a, b) and minimum (c, d) temperatures, respectively, with solid contours marking the temperature thresholds at which ice and NAT PSCs can form and the thresholds +2 K in the dashed lines. The thresholds +2 K are included to mark the possible increase of the formation temperatures by the Hunga $H_2O$ enhancement (Sect. 1.3). The use of 195 K and 188 K as a constant threshold for the two PSC types is a simplification for ease of presentation but the influence of altitude/pressure is considered when calculating the PSC areas (Sect. 2.2.2). For PSC analysis it is the minimum temperatures that are most relevant, however it is also useful to look at the average for each region as the minimum temperatures will be biased towards highest latitudes within the regions.

The core region experiences the coldest temperatures for the longest period of time. The minimum temperatures here reach the NAT PSC temperature threshold of 195 K by late April (Fig. 1c) followed by the average temperature in early May (Fig. 1a). The ice PSC threshold temperature of 188 K is reached by mid-May in the minimum and early June in the average. Near the end of the season, the ice threshold temperature is exceeded by mid-September in the average and early October in the minimum. The NAT threshold temperature is exceeded by late September in the average and October in the minimum, with some fluctuations as the season ends. The temperature thresholds for all types of PSCs are generally met in the core region in most years so PSCs form readily (subject to availability of $H_2O$ and $HNO_3$) and over relatively large areas resulting in very

https://doi.org/10.5194/egusphere-2026-3619
Preprint. Discussion started: 26 June 2026


efficient PSC processing. As such, the core region will typically experience large amounts of dehydration, denitrification, and heterogeneous chemical processing associated with the presence of these PSCs. The core region will also experience a longer period of polar night starting earlier and finishing later, therefore influencing the timing of any reactions that require sunlight (e.g. Roscoe et al., 2012).

The edge region is generally less cold and experiences shorter periods of time below the PSC thresholds than the core. The NAT PSC threshold temperature is met in the minimum by mid-May (Fig. 1d) and late July in the average (Fig. 1b). The ice PSC threshold is met in the minimum temperature by late-May but is not met in the average. At the end of the season ice occurrence ends in late September and NAT occurrence ends in mid-October, both with fluctuations. The temperatures in the edge region are less frequently below the PSC thresholds, and then for shorter periods meaning that PSCs and related processes are not as active as the core. As such, the ozone loss in the edge region is typically not as large and the processes do not tend to saturate, or reach levels as low as the core. The edge also experiences shorter periods in polar night and it is possible for portions to travel through sunlit areas as the vortex moves. This is a region that has little-to-no mixing with the core region, therefore acting as a dynamical ‘barrier’ that separates the air mass inside the vortex from the surrounding surf zone (Roscoe et al., 2012). When referring to this barrier the term "vortex boundary" will be used and the region is termed as "edge region". It is this vortex boundary that prevented the Hunga $H_2O$ enhancement from entering the majority of the vortex in 2022 prior to its break up in November 2022 (e.g. Manney et al., 2023). A further motivation to investigating the impact in the Antarctic edge region is the similarities of the environment to the Arctic stratospheric vortex in terms of the temperatures and PSC environment. The Arctic environment is less cold than the Antarctic, and drops below the ice PSC threshold less frequently, therefore experiencing less frequent PSCs with smaller areal extent. The ozone depletion in the Arctic does not reach the same extremes as the Antarctic. However, overall Arctic springtime ozone levels are very variable and there are examples of dynamically induced "mini holes" appearing with small areas of the Arctic stratosphere depleting below the 220 DU total column ozone level, such as seen in December 2019 and January 2020 (Kuttippurath et al., 2021).

#### 2.1.1 Quantifying the Antarctic vortex edge and core regions

There are three main methods to distinguish the stratospheric polar vortex from the surrounding surf zone with the aim of isolating distinct air masses. The simplest is to use geographical latitudes based on the polar cap or polar circle, however, this static definition will likely result in the merging of outside- and inside-vortex air. This definition may be reasonable to use for the Antarctic in midwinter as the vortex can be considered stable, circular and largely stays centred over the pole. It becomes less appropriate for investigations that break the vortex into structural regions, and when the vortex is establishing or breaking up. Therefore, a method that follows the movement of the vortex air masses is required to ensure that only the relevant air masses are captured (e.g Nash et al., 1996; Harvey et al., 2009). We use an equivalent latitude (EL) scheme based on the modified potential vorticity (PV) tracer calculated from a 3-D chemical transport model and compare our chosen boundaries to the PV contours using the steep gradient characteristic of the edge region to support our approach. The modified PV is used

https://doi.org/10.5194/egusphere-2026-3619
Preprint. Discussion started: 26 June 2026


to account for the variation of PV with altitude (Lait, 1994). For this study the core region is defined as $-90°$ to $-70°$ EL and the edge region as $-70°$ to $-55°$ EL to correspond with the steep gradient in PV.

### 2.2 Polar stratospheric clouds

#### 2.2.1 Polar stratospheric cloud chemistry

In autumn, before the PSCs form and heterogeneous chemical processing occurs, the majority of the inorganic chlorine in the lower stratosphere is the form of reservoir species HCl and $ClONO_2$ (Solomon, 1988; Wilmouth et al., 2006). The heterogeneous reactions occurring on or in the PSC particles convert the reservoir species into photolabile Cl-bearing species which when photolysed participate in reactions k1 to k6 (e.g. Seinfeld and Pandis, 2016; Solomon et al., 1986; Solomon, 1999). The process begins with the absorption of the HCl by the PSC particle setting up reaction k1 which releases the gaseous $Cl_2$ and retains the $HNO_3$ in the particle. For ozone depletion reaction k1 therefore performs two roles, first through the liberation of the $Cl_2$ which goes on to photolyse and release atomic Cl. Second, the removal of the $HNO_3$ from the system through the sedimentation of the NAT particle (denitrification) which prevents chlorine deactivation through the photolysis of the gaseous $HNO_3$ into $NO_x$ and thereby preventing reaction k4. Alongside reaction k1, k5 also contributes to the chlorine activation by producing HOCl which, when photolysed, releases Cl atoms that react with ozone in catalytic cycles, and produces $HNO_3$ which can contribute to denitrification. Denitrification, the removal of $HNO_3$, reduces the $NO_x$ concentrations in the vortex environment, allowing the active chlorine species to remain elevated until later in the season thereby enhancing ozone depletion (e.g. Solomon, 1999; Davies et al., 2002). With arrival of the sunlight, the photolysis of the remaining gas phase $HNO_3$ leads to an increase in $NO_2$ which then reacts with the ClO to reform $ClONO_2$. Denitrification in the Antarctic does not always have the same bearing on the magnitude of ozone depletion as in the Arctic (Davies, 2003) and it is possible that due to the lower likelihood of saturation and therefore lower ozone depletion, the edge region may be more influenced by denitrification. Similarly to the denitrification by NAT particles, the ice particles will also sediment and remove the $H_2O$ (dehydration). Both denitrification and dehydration are partnered with renitrification and rehydration at lower altitudes where the PSC particles are no longer supported and evaporate (e.g. Solomon, 1999; Jensen et al., 2002).

$$\begin{aligned}
HCl(s) + ClONO_2 &\xrightarrow{k1} Cl_2 + HNO_3(s)\\
Cl_2 + h\nu &\xrightarrow{k2} 2\,Cl\\
2[Cl + O_3 &\xrightarrow{k3} ClO + O_2]\\
ClO + NO_2 + M &\xrightarrow{k4} ClONO_2 + M
\end{aligned}$$

---

$$\text{Net: } HCl(s) + NO_2 + 2\,O_3 \longrightarrow ClO + HNO_3(s) + 2\,O_2$$

---

$$\begin{aligned}
ClONO_2 + H_2O(s) &\xrightarrow{k5} HOCl + HNO_3(s)\\
HOCl + HCl(s) &\xrightarrow{k6} Cl_2 + H_2O
\end{aligned}$$

https://doi.org/10.5194/egusphere-2026-3619
Preprint. Discussion started: 26 June 2026


(s, indicates a species on the PSC particle surface)

#### 2.2.2 Calculating polar stratospheric cloud areal extent

We calculate the polar stratospheric cloud areal extent ($A_{PSC}$) based on the thermodynamic equilibrium assumption with the gas phase. The threshold concentrations (saturation pressures) required for PSCs formation are computed for values of $HNO_3$ and $H_2O$ using the formula from Hanson and Mauersberger (1988) for relevant temperatures and pressures. Once the thresholds were calculated, we determined whether ice or NAT PSCs are possible using the modelled $H_2O$ and $HNO_3$ number densities. NAT is assumed to form if the $HNO_3$ number density is greater than 10 times the saturation threshold for NAT and Ice particles will form if the $H_2O$ number density is greater than the saturation threshold for ice (e.g. Fahey et al., 2001; Drdla et al., 2002).

## 3 Model and Observations

### 3.1 TOMCAT 3-D chemical transport model description

The TOMCAT/SLIMCAT global-3D chemical transport model (hereafter TOMCAT) is described in Chipperfield et al. (1993, 1996); Chipperfield (2006). Here simulations are performed at a horizontal resolution of 2.8° × 2.8° with 32 vertical levels extending from the surface to about 60 km. The model is forced by meteorological reanalysis data from the ECMWF ERA5/5.1 dataset (Hersbach et al., 2020). TOMCAT incorporates a detailed gas-phase stratospheric chemistry scheme and uses time-varying mixing ratios of ozone depleting substances and greenhouse gases from World Meteorological Organization (WMO). (2022) as surface boundary conditions. Time-varying solar irradiance changes are from NRL solar irradiance model (V2) (Coddington et al., 2019) and updated until December 2024 (e.g. Dhomse et al., 2016). For stratospheric aerosol surface area density (SAD) the model uses the so-called 3$\lambda$ data from Arfeuille et al. (2014) as described in Dhomse et al. (2015), but from January 2017 onwards, the model uses SAD data from Knepp et al. (2024). Essentially, these SAD values are derived from the SAGE-III multi-wavelength aerosol extinction measurements at 453, 525, and 1020 nm. In this paper, the model uses a simplified representation of PSCs. For heterogeneous reactions on PSCs and the rates of dehydration and denitrification the model assumes the thermodynamic equilibrium between the surrounding gas phase (e.g. Feng et al., 2011) and the three main types of PSC particles considered, namely nitric acid trihydrate (NAT), supercooled ternary solution (STS), and ice. The PSC scheme assumes the sedimentation of the ice particles based on a radius of 10 $\mu$m with a 1500 m/day fall velocity.

The model simulation setup used here is similar to that used in Zhou et al. (2024) and Chipperfield (2025). An important update since Zhou et al. (2024) and also used in Zhou et al. (2026) is that $H_2O$ entry mixing ratios now include an annual cycle near the tropical tropopause region, rather than the previous setup where model had fixed annual mean entry mixing ratio. Here, we analyse daily output sampled at 1:30 pm local time that is close to NASA's Aura equator crossing time to allow for direct comparisons with Microwave Limb sounder (MLS) measurements. A control model simulation (Control_G ) starts in 1979, and is used to initialise all other sensitivity simulations through the Hunga period. For the simulations which include $H_2O$, we inject 150 Tg of $H_2O$ between 2°S to 28°S latitudinally and vertically between 22 km and 26 km on April 1$^{st}$. The timing of the $H_2O$ injection is described in Zhou et al. (2024). This approach aims to represent impacts from ∼80 days after

https://doi.org/10.5194/egusphere-2026-3619
Preprint. Discussion started: 26 June 2026


the eruption, once the initial radiatively-forced descent phase (Sellitto et al., 2022) had stabilised with the initial plume fully dispersed zonally, with well-mixed and dilute $H_2O$ and aerosol layers (e.g. Legras et al., 2022).

### 3.2 Model simulations and experiments

We performed four model experiments to investigate the Hunga impact from the $H_2O$, stratospheric aerosol, and combined impact (Table 1). For the bulk of this paper we focus on the ΔWater_Vapour simulations, Control_G and Hunga_H2O . Within the experiments, we employ two methods of representing the stratospheric aerosol: SAGE III SAD and repeating 2017 SAD, chosen as a year with relatively clean background conditions without perturbations from volcanic eruptions or wildfires. This allows for the inclusion of a 'clean' control without Hunga inputs by repeating the 2017 SAD conditions. All simulations were integrated until March 2025, but this paper focusses on the period April to December 2023. We use "simulations" to refer to individual model runs and "experiments" to refer to the difference of 2 simulations that are used to create a delta (Δ), i.e. perturbed simulation − control simulation. The simulations are described in Table 1 and experiments in Table 2.

Experiment ΔWater_Vapour focusses on the $H_2O$ enhancement impact alone. The ΔAerosol_noH2Ointeraction experiment allows for the investigation of the aerosol impact without any interactions with the Hunga $H_2O$ enhancement. The ΔAerosol_H2Ointeraction is the same as ΔAerosol_noH2Ointeraction but with the Hunga $H_2O$ in both simulations to show the interaction between the aerosol and water, still focussing on the aerosol impact. Finally, we use a 'clean' control to simulate the combined impact of the $H_2O$ and sulfate aerosols for ΔCombined . This paper primarily focuses on the contribution of the $H_2O$ to the ozone depletion using the ΔWater_Vapour experiment, rather than the stratospheric aerosol or the combined impact but we do compare the ozone responses between all the experiments in Sect. 5.2.

| Simulation name | $H_2O$ | Hunga stratospheric aerosol |
|---|---|---|
| **Control_G** | No | Yes (SAGE III) |
| **Hunga_H2O** | Yes | Yes (SAGE III) |
| **Clean** | No | No (Repeating 2017 SAD) |
| **Clean_H2O** | Yes | No (Repeating 2017 SAD) |

**Table 1.** Summary of the four TOMCAT simulations used in this study to quantify effects of the water vapour and stratospheric aerosol enhancements.

### 3.3 Observations - NASA Aura Microwave Limb Sounder

We compare the TOMCAT model results to the NASA Aura Microwave Limb Sounder (MLS) V5 data as it provides stratospheric measurements for the majority of the polar regions (82°N and 82°S) including during polar night (Waters et al., 2006). We use vertical profiles (level 2) of $O_3$, HCl, $H_2O$, $HNO_3$, and ClO alongside daily binned level 3 (ML3DB) constructed by the MLS team at NASA/JPL. These involved re-gridding the native level 2 along-track measurements to different coordinate systems to simplify analysis of transport and chemistry process. These processed datasets include zonal-mean averages of MLS

https://doi.org/10.5194/egusphere-2026-3619
Preprint. Discussion started: 26 June 2026


| Target impact | Simulations used | Experiment label |
|---|---|---|
| Impact of Hunga $H_2O$ | 1. Hunga_H2O - Control_G | **ΔWater_Vapour** |
| Impact of Hunga stratospheric aerosol | 2. Control_G – Clean<br>3. Hunga_H2O – Clean_H2O | **ΔAerosol_noH2Ointeraction**<br>**ΔAerosol_H2Ointeraction** |
| Combined impact | 4. Hunga_H2O – Clean | **ΔCombined** |

**Table 2.** Summary of the experiments based on the difference between two model simulations with different water vapour and stratospheric aerosol. Each experiment is categorised under one of three target impacts to investigate.

species resolved on a potential temperature ($\theta$) vs. EL grid to ensure comparisons between the two vortex regions in both the model and observations are correctly distinguishing between the relevant air masses.

## 4 Results and Discussion

### 4.1 Transport of Hunga-excess water vapour

The results in Sect. 4 are discussed in the context of experiment ΔWater_Vapour , therefore focussing on the impact of the $H_2O$ enhancement. Comparison with MLS observations shows that the TOMCAT Hunga_H2O captures the vertical profile and timing of the dehydration in 2023 well (Fig. 2c-f). The $H_2O$ mixing ratio (vmr) in Hunga_H2O is enhanced by ∼2.5 ppm across the vortex increasing the vmr to ∼7.5 ppm by the start of 2023 relative to Control_G (Fig. 2c-d). The core presents as a vertically thin layer with a gradient from lower values at the higher levels to the highest values towards the base of the band (Fig. 2a). The highest values in this band start between 650 K and 475 K in April and descend to between 550 K and 450 K by early June with the vertical structure of the enhancement being maintained. After early June, the $H_2O$ enhancement in the core rapidly reduces to ∼0 following strong removal (yellow line; Fig. 2 d, e). As such, for the core, only the first ∼25.55% of the overall April-December vortex season is enhanced by the Hunga $H_2O$. The $H_2O$ begins to gradually return from the higher levels in August but does not enter the contours marking the PSC temperature thresholds. In the edge region, the Hunga $H_2O$ presents as a vertically deeper layer of enhancement, extending from >750 K to 475 K in April. This enhancement descends over time with the upper boundary moving the higher values to below 650 K and the lower boundary towards 450 K. The maximum enhancement is less defined and more evenly spread than in the core (Fig. 2b). After early July, the enhancement shows a slight stepped decrease from ∼2.5 ppm to ∼1 ppm which is maintained, with some fluctuations, through the remainder of the season. This decrease is later, less steep, and not as defined as the core.

The stepped decrease in the $H_2O$ in both regions (core in June, edge in July) is a marker of PSC appearance. Large ice PSC particles remove the $H_2O$ from the vortex via dehydration as they sediment to lower levels. This mechanism of removal has been highlighted as the main initial removal mechanism for the Hunga $H_2O$ enhancement in 2023 (Zhou et al., 2024). However, due to the differences in the conditions in the two regions the efficiency of this dehydration varies. The core, being much colder, typically experiences very effective dehydration which primarily drives the sudden near-total removal of the

https://doi.org/10.5194/egusphere-2026-3619
Preprint. Discussion started: 26 June 2026


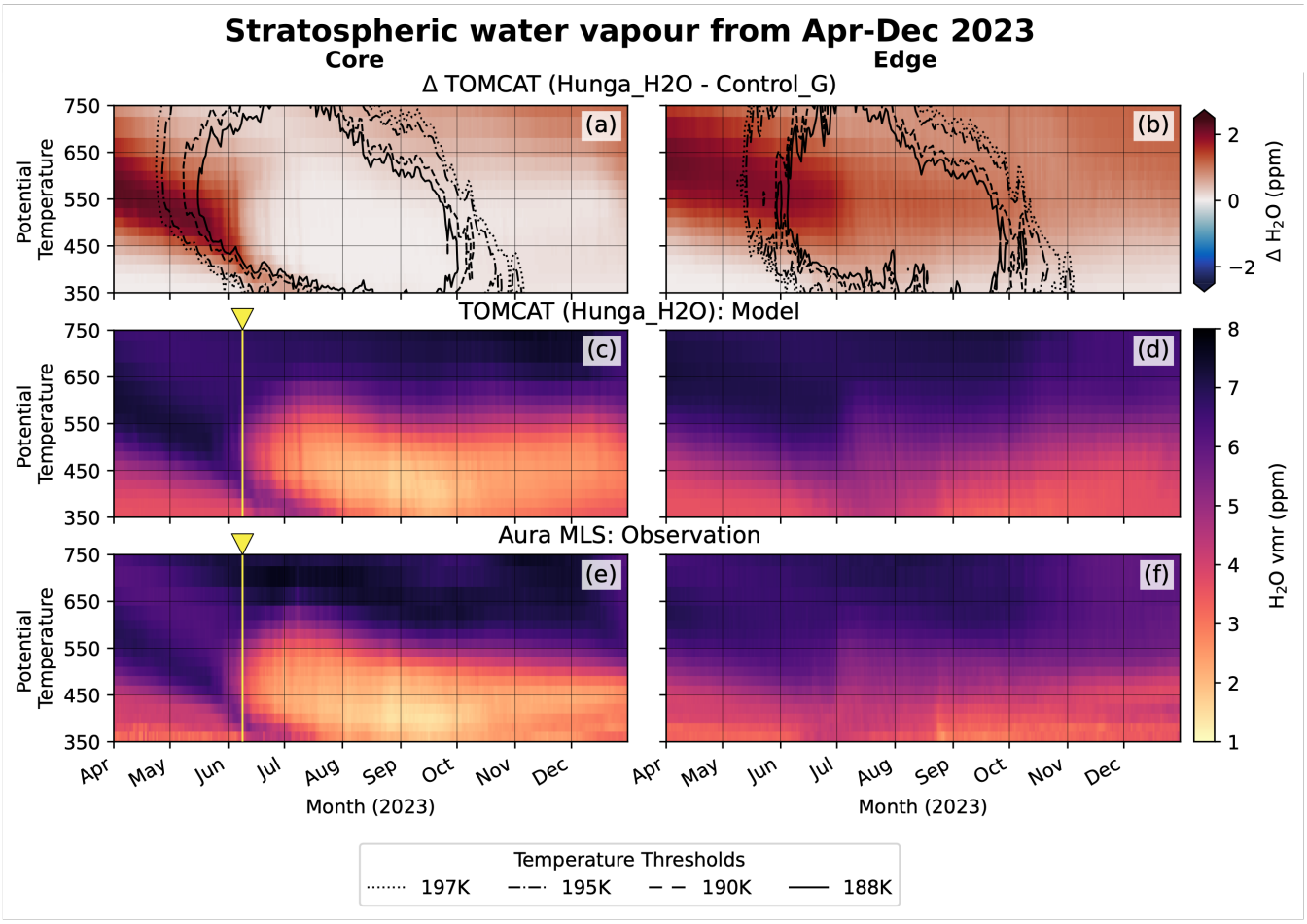


**Figure 2.** Hunga $H_2O$ enhancement from 1st April 2023 to 31st December 2023. Panels (a) and (b) show the Δ Hunga_H2O (with Hunga $H_2O$ injection) − Control_G (without $H_2O$ injection) overlaid with contours indicating the PSC threshold temperatures for NAT (195 K) and ice (188 K) as solid lines. Dashed lines mark the threshold temperatures +2 K. Panels (c) and (d) show the modelled mean (area-weighted) volume mixing ratio of the Hunga_H2O simulation. Panels (e) and (f) show the observed $H_2O$ volume mixing ratio from the MLS instrument. Panels (a)-(b) and (c)-(f) use the same colour scales. The left panels are for the core region (−90° to −70° EL) and right are for the edge (−70° to −55° EL). Yellow lines and triangles mark the point of near-complete removal of the Hunga $H_2O$ enhancement.

Hunga $H_2O$ enhancement. In contrast, the edge is not as cold and generally has less extensive PSCs. Therefore, the PSCs do not remove the $H_2O$ as effectively as in the core, leaving the remaining ∼1 ppm enhancement in the edge after early July.

### 4.2 Impact on polar stratospheric cloud extent

The PSC areal extent ($A_{PSC}$) for NAT and ice in both vortex regions is increased in the Hunga_H2O simulation with the magnitude of the change due to both the earlier appearance and increase in magnitude, especially at the beginning and end of

https://doi.org/10.5194/egusphere-2026-3619
Preprint. Discussion started: 26 June 2026


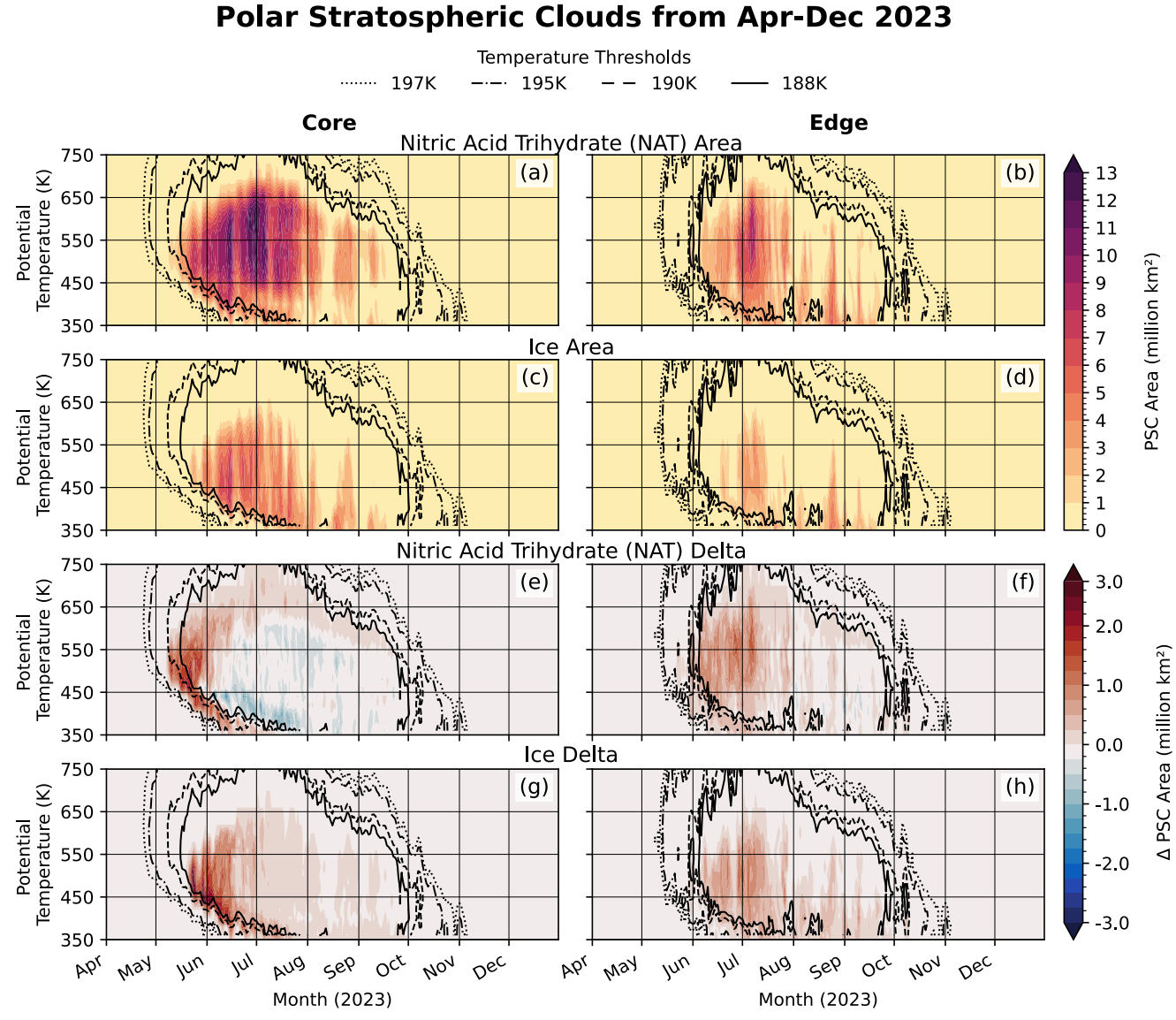


**Figure 3.** Modelled PSC extent estimated from the TOMCAT output. NAT (panels (a) and (b)) and ice (panels (c) and (d)) PSC extent are from Control_G . Panels (e)-(h) show the differences in PSC areal extent (Hunga_H2O – Control_G ) for NAT ((e) and (f)) and ice ((g) and (h)). For all panels, the 195 K NAT (dot dashed) and the 188 K ice (solid) temperature thresholds are marked. These thresholds +2 K are marked as dashed (190 K) and dotted (197 K). The left panels are for the core region ($-90°$ to $-70°$ EL) and right are for the edge ($-70°$ to $-55°$ EL).

the season (Fig. 3e-h). This is due to the additional $H_2O$ is promoting the formation of PSCs at slightly higher temperature

https://doi.org/10.5194/egusphere-2026-3619
Preprint. Discussion started: 26 June 2026


thresholds. The $\Delta A_{PSC}$ values for both the ice and NAT PSCs vary between the two regions, initially due to the difference in the temperature regimes.

The differences in the NAT and ice $\Delta A_{PSC}$ in the core region are mostly concentrated towards the beginning of the season (Fig. 3e & g). The NAT clouds show a pattern of initially large increased $A_{PSC}$ at the beginning of the season but this changes to negative from June. The largest period of NAT increase occurs during May, then becomes negative and fluctuates around zero, except above 650 K. The largest decreases in the NAT occurs beneath the 450 K level between June and August with smaller negative values scattered above for the remainder of the season (Fig. 3e). The change from positive to negative $\Delta A_{PSC}$ in the NAT extent occurs is an indication of ice formation consuming the excess $H_2O$ (Fig. 3g). When the ice clouds begin to form and remove the excess $H_2O$ by dehydration, the impact from the Hunga $H_2O$ on NAT is decreased. For the ice clouds, the largest period of increase occurs from mid-May to mid-June with a small increase around 0.2 million km$^2$ that fluctuates towards 0 for the rest of the season after the excess $H_2O$ is removed (Fig. 2a).

The differences in $A_{PSC}$ values in the edge region have less of a contrast over the season (Fig. 3f & h). The peak $\Delta A_{PSC}$ for both the NAT and ice PSCs occur between mid-May and mid-July with the increase towards and after these peak areas more gradual than the core. This reflects the differences in the temperature regimes where the periods below the PSC threshold temperatures are shorter and fluctuate more in the edge than in the core. The $\Delta A_{PSC}$ of both the ice and the NAT clouds in the edge vary but generally maintain a positive value until August followed by fluctuations around zero up to October. The maintenance of the positive $\Delta A_{PSC}$ is likely due to the much lower abundance of ice in the edge region, and therefore less effective dehydration (Fig. 2b), which is determined by the temperature differences. Alongside dehydration by ice PSCs, dentrification by NAT PSCs will also contribute by removing $HNO_3$ and some $H_2O$.

### 4.3 Additional denitrification

Comparison with MLS observations shows that the TOMCAT Hunga_H2O simulation captures the vertical profile of the $HNO_3$ reasonably well in the core but with a high bias above 650 K between May and October (Fig. 4e-h). The edge also agrees relatively well with the MLS observations but with a slight low bias from July onwards. These biases are consistent with those documented and discussed in Feng et al. (2011). The average modelled $\Delta HNO_3$ due to Hunga in both the edge and the core are similar to the PSC changes (Sect. 4.2). Figure 4c shows the largest change to the $HNO_3$ in the core at the beginning of the season in early May as a decrease of around 1 ppb at 550 K accompanied by an increase of a similar scale around the 475 K level. This increase frames the bottom of the decrease as a narrow band descending until mid-June and is an indication of re-nitrification. The decrease begins gradually between 550 K and 500 K increasing in magnitude to a maximum average of 2.3 ppb and vertical extent to between 375 K and 650 K in early June. The $\Delta HNO_3$ then returns to near 0 from the beginning of June following the same shape as the start. The $\Delta HNO_3$ within the edge region, however, does not show this initial large spike, beginning later and with a lower magnitude than the core, reflecting the differences in the PSC environment and temperatures between the two regions.

For the overall vertical profiles, the negative $\Delta HNO_3$ start at the higher levels of the vortex and are mirrored by positive $\Delta HNO_3$ on the lower levels (Fig. 5). The PSC temperature thresholds are reached at the lower levels as the season progresses

https://doi.org/10.5194/egusphere-2026-3619
Preprint. Discussion started: 26 June 2026


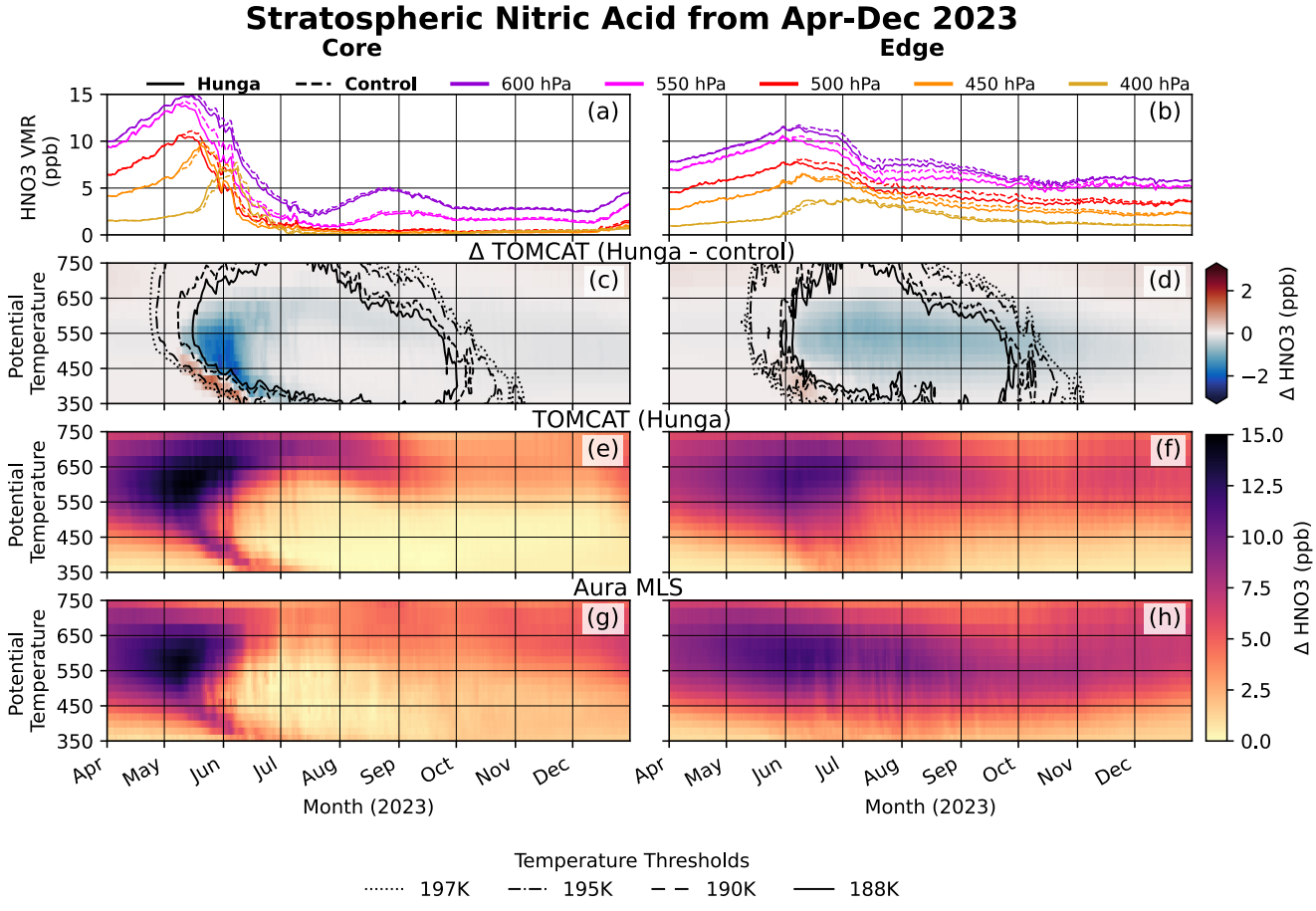


**Figure 4.** Modelled and observed $HNO_3$ from 1st April 2023 to December 31st 2023. Panels (a) and (b) show the model simulations Hunga_H2O (solid) and Control_G (dashed) for five selected pressure levels to show the decrease at the beginning of the season and difference in behaviour between the regions. Panels (c) and (d) show vertical profiles of the deltas for simulations Hunga_H2O − Control_G as means for the core (left) and edge (right) regions overlaid with contours indicating the PSC threshold temperatures for NAT (195 K) and ice (188 K) as solid lines. Dashed lines mark the threshold temperatures +2 K. Panels (e) and (f) show the $HNO_3$ vmr in the simulation Hunga_H2O . Panels (g) and (h) show the MLS observed $HNO_3$.

and the negative $\Delta HNO_3$ follows, eventually removing any positive $\Delta HNO_3$ caused by the re-nitrification. As these initial stages progress the impact reduces from the upper levels over time with 500 K showing the strongest negative impact from the excess Hunga $H_2O$ and 450 K showing the strongest re-nitrification behaviour alongside denitrification once it begins. The pattern of increase follows the NAT temperature contours until the denitrification bottoms out the $HNO_3$ in the core (Fig. 4a), and as the ice PSCs begin to appear. Therefore, it is possible the efficiency of the typical PSC behaviour in the core is limiting

https://doi.org/10.5194/egusphere-2026-3619
Preprint. Discussion started: 26 June 2026


the magnitude of the impact to the denitrification through a combination of the $HNO_3$ stabilising by reaching zero and the additional removal of $H_2O$.

The formation of NAT PSCs and the associated denitrification begins as a small area within the upper levels of the vortex core and expands to the lower levels and more widely across the vortex as the season progresses, making it interesting to look beyond the averages (Fig. S5, S6). From experiment ΔWater_Vapour there are three structures to the $\Delta HNO_3$: An initial cohesive, rounded segment in the middle of the core region, within the NAT temperature contours, with a $\Delta HNO_3$ of $-5$ ppb. This sits vertically between 600 K and 500 K in mid-May and is accompanied by a vertically thinner area of positive $\Delta HNO_3$ between 480 K and 425 K of 3.6 ppb. This positive $\Delta HNO_3$ sits at the very bottom and below the NAT temperature contours strongly indicating increased denitrification and re-nitrification. Both the positive and negative $\Delta HNO_3$ show the highest values in the middle which dissipate outwards but remain within the core in this initial period. As the vortex moves into early-June, the NAT temperature thresholds start to extend into the edge region. The $\Delta HNO_3$ follows the expansion of the thresholds but it is no longer a cohesive segment and begins to take on a loop/ring like shape bordering the core region and beginning to enter the edge region. In this second stage the $\Delta HNO_3$ has reduced substantially (moved towards 0) in the centre of the ring where the initially largest values were. The positive $\Delta HNO_3$ in this second stage follows the horizontal extent of the negative but has vertically narrowed and the $\Delta HNO_3$ has reduced (Fig. 5). The third stage of the $\Delta HNO_3$ becomes a ring of negative moving out to eventually become confined to the edge region with very small values within the core by July, after which the $\Delta HNO_3$ remains fairly constant at $\sim$1 ppb until mid-October when the vortex becomes unstable.

Consequently, the TOMCAT ΔWater_Vapour shows Hunga has created an environment with an increased areal extent and prolonged duration of NAT PSCs meaning the scale of the denitrification is increased, allowing for a longer period of reactions between ClO and $O_3$ before the reformation of the reservoir species occurs. This is where the differences between the edge and the core region environments play an important role. The core region deactivation of $ClO_x$ is primarily influenced by the typically very efficient PSC processing leading to almost complete removal of the $HNO_3$ (like the $H_2O$) and very low $O_3$ concentrations in a typical year. Therefore, the earlier formation and increased areal extent of the NAT clouds only have an effect at the beginning of the season until the $HNO_3$ bottoms out, limiting the impact to the $HNO_3$ and other related processes after that point. In contrast, the edge region's PSC environment is far less efficient and the $HNO_3$ does not bottom out, allowing a longer period of $HNO_3$ decrease, although not as large in magnitude.

### 4.4 Additional chlorine activation

The pattern and shape of the relationship between the reservoir and active species is preserved within both Hunga_H2O and Control_G simulations (Fig. 6). As the PSCs start to form in mid-May the reservoir species decline fairly rapidly up to June/July, and the active species gradually increase (Fig. 6a-b). Figure 6c - h focusses on ClO as a representative for the active species, and HCl and $ClONO_2$ for the reservoir species as area-weighted means for the two regions.

The core region (Fig. 6, left column) generally exhibits the largest impact at the beginning of the season and a final peak at the end. The reservoir species in the core region show an initial decrease at the beginning of the season between mid-May to mid-June typically reaching very low values quickly. The $\Delta HCl$ reaches a maximum reduction of $-0.5$ ppb in June (Fig. 6e)

https://doi.org/10.5194/egusphere-2026-3619
Preprint. Discussion started: 26 June 2026


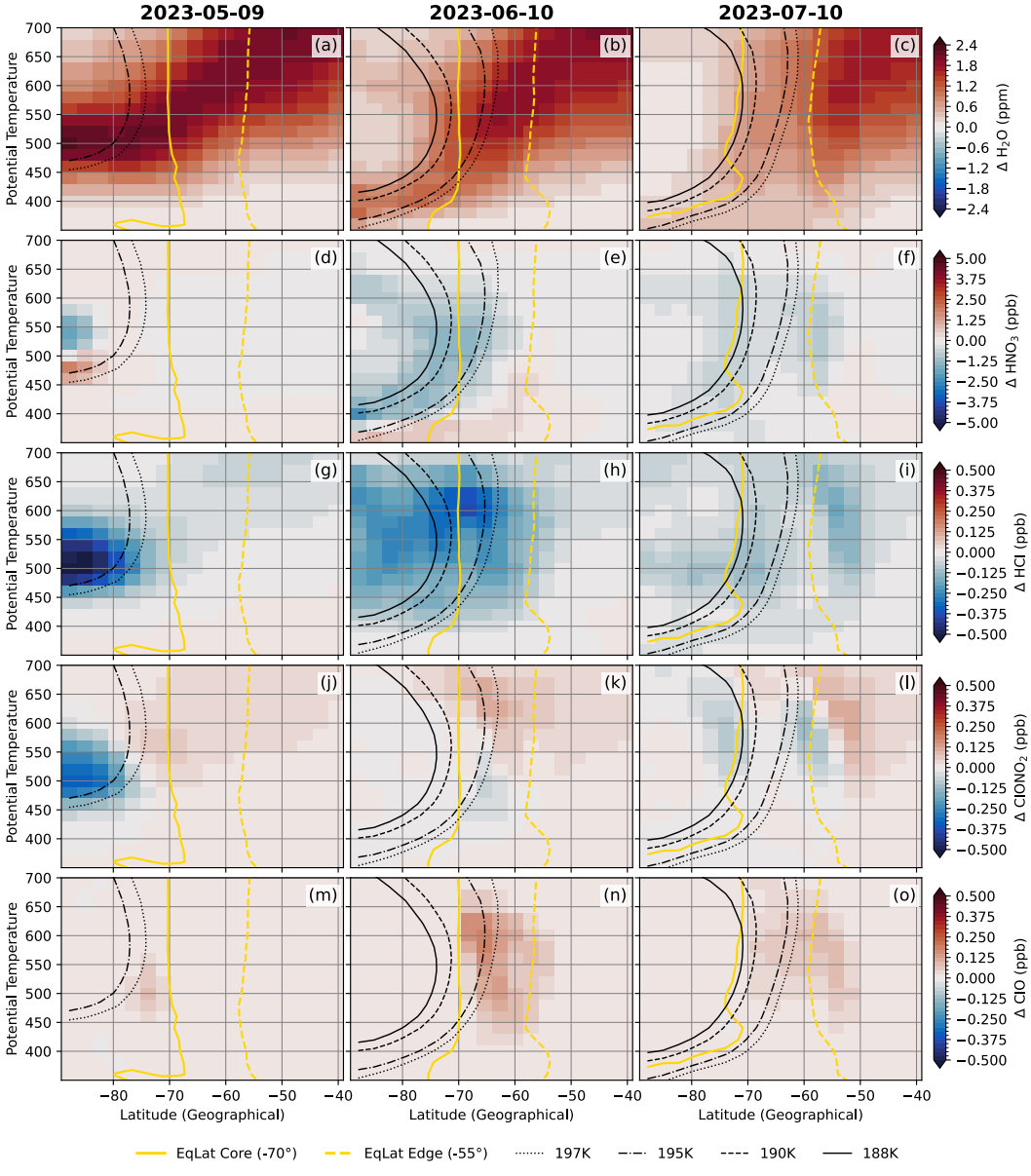


**Figure 5.** Vertical cross sections (geographical latitude versus potential temperature) of 3 example days during the initial period of PSC appearance chosen to highlight the de(re)nitrification. The rows show the modelled TOMCAT CTM Δ for (a)-(c) $H_2O$, (d)-(f) $HNO_3$, (g)-(i) HCl, (k)-(l) $ClONO_2$, and (m)-(o) ClO. Δ is calculated as Hunga_H2O (with $H_2O$ injection) – Control_G (without injection). Panels are overlaid with contours highlighting the PSC threshold temperatures for the NAT (195 K) in purple and ice (188 K) in grey. Dashed lines mark the threshold temperatures +2 K. Black contours mark the equivalent latitude boundary for the core (solid, −70°) and dashed, the edge (dashed, −55°).

https://doi.org/10.5194/egusphere-2026-3619
Preprint. Discussion started: 26 June 2026


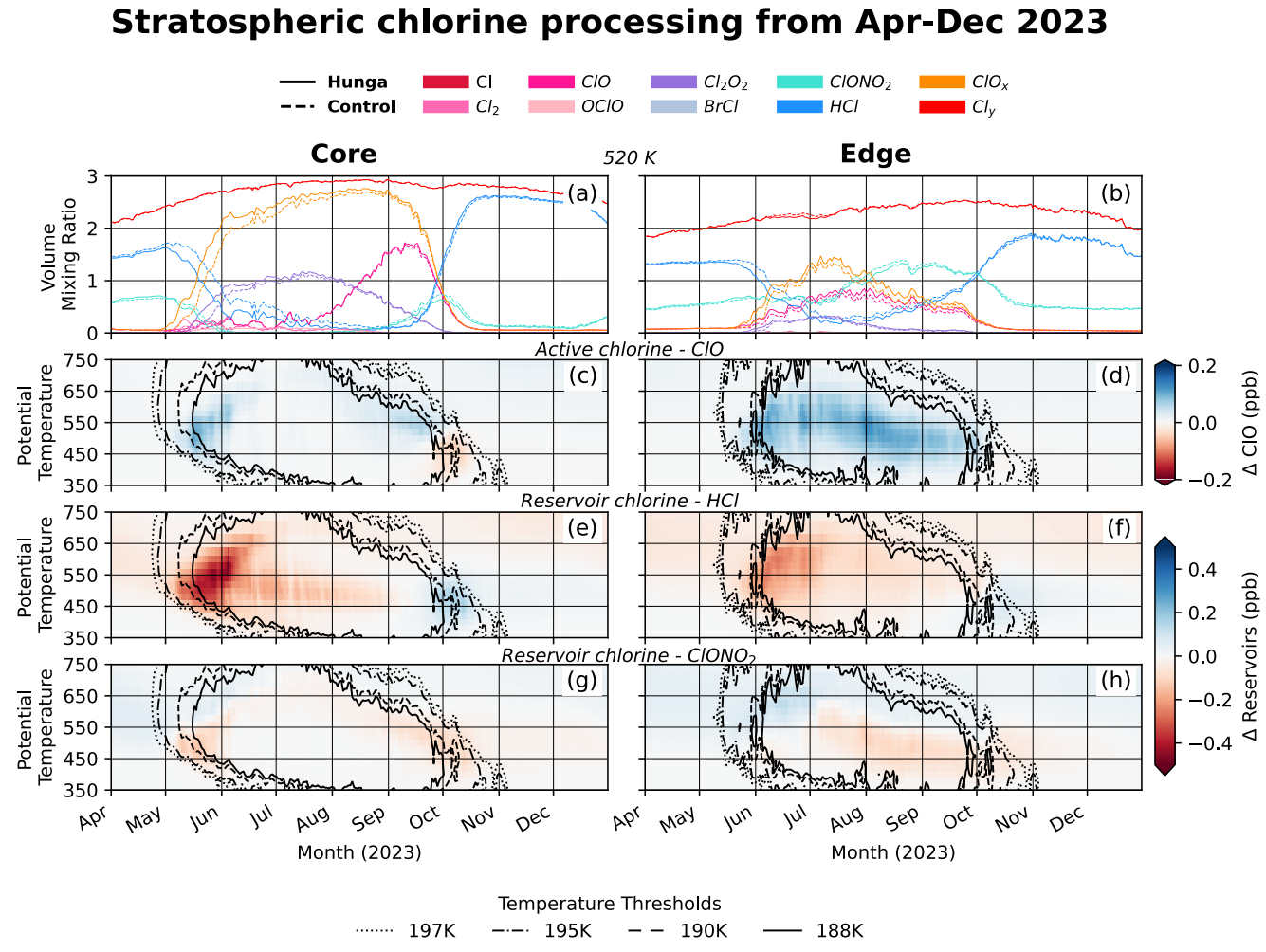


**Figure 6.** Modelled TOMCAT CTM chlorine species from 1st April to December 31st 2023. Panels (a) & (b) show the area-weighted mean of the main chlorine species in the $Cl_y$ family on the 520 K isentropic level to highlight the relationship between the reservoir and active species. The Hunga_H2O simulation (with $H_2O$ injection) uses solid lines and Control_G (without injection) uses dashed lines. The species shown are Cl, $Cl_2$, ClO, OClO, $Cl_2O_2$, BrCl, $ClONO_2$, HCl, $ClO_x$, and $Cl_y$. Panels (c)-(h) are vertical curtains of the deltas from Hunga_H2O − Control_G as means for the core (left) and edge (right) regions for (c)-(d) ClO, (e)-(f) HCl and (g)-(h) $ClONO_2$. Panels (c)-(h) are overlaid with contours highlighting the PSC threshold temperatures for the NAT (195 K) and ice (188 K) in the minimum temperatures as solid lines. Dashed lines mark the threshold temperatures +2 K.

and $\Delta ClONO_2$ reaches a maximum reduction of −0.15 ppb in mid-May (Fig. 6g). The $ClONO_2$ is reduced to the lowest point by early-June and remains there with very little fluctuation until it begins reforming from mid-August. The HCl also rapidly declines from mid-May until early June to concentrations around 0.5 ppb, after which the gradient is significantly reduced and the vmr slowly decreases towards the lowest point in mid-August until it rapidly increases as the HCl is reformed from

https://doi.org/10.5194/egusphere-2026-3619
Preprint. Discussion started: 26 June 2026


mid-September. The HCl in the Hunga_H2O experiment begins this rapid reduction earlier and with an increased magnitude, reaching lower values at the end of the initial decline than the Control_G before the gradient was reduced. The magnitude of the difference in the HCl between the Control_G and Hunga_H2O experiments is somewhat maintained through the initial rapid decline, but once the gradient has reduced after June the difference between the two decreases as they approach very low concentrations.

The reservoir species in the edge region behave similarly to the core where the decline begins earlier in the Hunga_H2O simulation and there is an overall reduction in the concentration (Fig. 6, right column). However, unlike the core, the edge maintains the reduction throughout the season. The $\Delta$HCl in the edge region does exhibit an initial peak of decline at the beginning of the season of up to $-0.3$ ppb but this reduces more gradually, and a small amount of additional loss is maintained until HCl begins to reform (Fig. 6f). The $ClONO_2$ in the edge region has a much less distinct reduction than seen in the core and the reduction is initially small in June, increasing after July up to a maximum $\Delta ClONO_2$ of $-0.14$ ppb (Fig. 6h), similar scale to the core.

The active chlorine species, as with the reservoirs, in the core region show initial changes at the beginning and the end of the season (Fig. 6c). In the core, there is an initial increase reaching a maximum $\Delta$ClO of 0.11 ppb between May and June starting between the 450 K and 570 K levels and arcing up into the higher levels gradually reducing into mid-June. The increase reappears at the higher levels from mid-July, becoming larger as it descends towards late-September. The $\Delta$ClO changes to negative between late-September and early-October around the temperature fluctuations at the end of the season. In the edge region, the $\Delta$ClO is increased persistently by up to 0.13 ppb through the season as a band initially starting between 650 K and 450 K, descending towards 550 K and 450 K by early-August (Fig.6b), and does not show the period of reduction in October seen in the core.

The individual changes to the active chlorine species involved in the heterogeneous chlorine reactions are reflected in the impact to $ClO_x$ (= Cl + ClO + $2Cl_2O_2$) (Fig. 6a-b, yellow lines). The core shows an initial large change to the $ClO_x$ at the beginning of the season starting from May. As the season progresses, the difference becomes less and the season ends with a small increase. In contrast, the edge shows an initial increase that is maintained throughout the season at a similar magnitude until October. The pattern of fluctuations appears in both simulations with the magnitude being the main difference.

The influence of the Hunga $H_2O$ enhancement on the heterogeneous chlorine reactions reflects the PSC response, with an earlier start, a small decrease to the reservoirs and increase to the active species. The main difference in the impact between the two regions is the longevity of the changes during the season. The edge region experiences changes throughout the season while in the core changes are generally focussed at the beginning and the end. The PSCs in the core region are limited by the efficiency of the dehydration by the ice PSCs and denitrification by the NAT, therefore once the $\Delta A_{PSC}$ in the core is reduced to 0 or negative values, the impact on the chlorine species also diminishes. This impact is especially evident in the ClO in the core (Fig. 6c), where the first period of increase follows the shape of the NAT $\Delta A_{PSC}$, supporting the link between the PSC behaviour and the appearance of the active species. This is demonstrated through the differences between the two vortex regions. The edge region does not reach the very low levels as readily as the core and maintains a reduction in reservoir species throughout the season, whereas the reduction in the core region decreases and stops as the concentrations approach 0. As such,

https://doi.org/10.5194/egusphere-2026-3619
Preprint. Discussion started: 26 June 2026


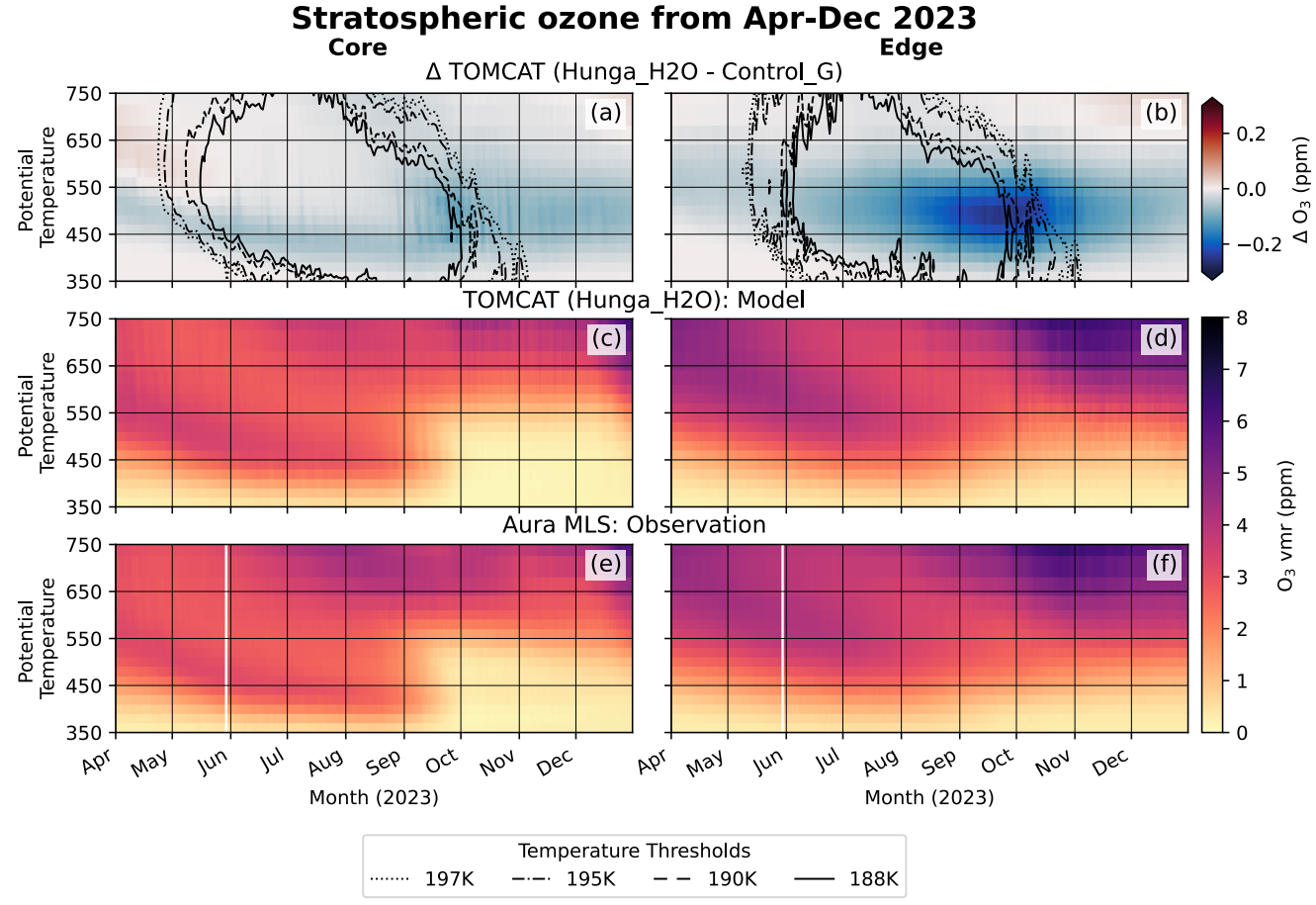


**Figure 7.** Ozone differences ($\Delta O_3$) and volume mixing ratios (vmr) in parts per millions (ppm) from 1st April to December 31st 2023. Panels (a) & (b) show the $\Delta O_3$ from Hunga_H2O (with $H_2O$ injection) − Control_G (without injection) overlaid with contours indicating the PSC threshold temperatures for NAT (195 K) and ice (188 K) as solid lines. Dashed lines mark the threshold temperatures +2 K. Panels (c) & (d) are the modelled $O_3$ vmr of the Hunga_H2O model run as a area weighted mean. Panels (e) & (f) show the MLS observations. Panels (b)-(e) use the same colour scale. The left panels are for the core region (−90° to −70°EL) and right is the edge (−70° to −55° EL).

we suggest the influence of the Hunga $H_2O$ enhancement on the chlorine processing is limited by both the efficiency of the ice PSCs to dehydrate, the chlorine processing in the core leading to saturation, and the reservoir species reaching and remaining at zero. These factors do not have as much of a limiting impact in the edge region as the PSCs are not as effective.

### 4.5 Additional chemical ozone depletion

Comparison with MLS observations shows that the TOMCAT Hunga_H2O simulation captures the magnitude and timing of the ozone behaviour in the April to December 2023 period well (Fig. 7). In both vortex regions additional ozone depletion due

https://doi.org/10.5194/egusphere-2026-3619
Preprint. Discussion started: 26 June 2026


to Hunga began before the start of 2023, with small amount of ozone loss of up to −0.05 ppm preceding the 2023 vortex season. This initial loss in the core is present as a narrow band starting in April between 550 K and 450 K that descends through to late-August (Fig. 7a), paired with a small (−0.03 ppm) ozone increase above 550 K. The initial loss in the edge region is vertically taller and smaller in magnitude (0.002 ppm), with the ozone increase at higher levels appearing in November/December (Fig. 7b). Figure 7a shows that the additional ozone depletion during the main ozone loss period in the core begins gradually from September, mainly between the 370 K and 550 K levels. The peak in the additional depletion in the core reaches −0.12 ppm on August 24th. Figure 7b shows the additional loss in the edge region as longer and more defined than the core, reaching a maximum of −0.26 ppm on August 22nd. The maximum period of additional ozone depletion in the edge occurs between August and November, primarily between the 400 K and 600 K levels.

The difference in timings of the ozone depletion between vortex regions is likely to be driven by the availability of sunlight and the edge moving rather than the $H_2O$ enhancement. However, the greater magnitude of the loss in the edge region is driven by the greater ClO increase, alongside the efficiency of the typical ozone depletion in the core region. The core region experiences a period of additional HCl increase coupled with a ClO decrease during October as the ozone depletion cycles come to an end as active chlorine reforms HCl in a regime of near-zero ozone. Although the ozone depletion in the edge is not as efficient, low ozone values are observed in the edge region, but for a much briefer period and smaller areas. There is also a small increase in the HCl in the edge at the end of the season, but it is less defined than the core (Fig. 6e-f).

## 5 Implications and broader context

### 5.1 Chemically driven earlier and larger Antarctic ozone hole

Previous volcanic eruptions have been known to increase the Antarctic ozone hole area. For example, eruptions in 2006, 2007, and 2008 are estimated, from global model simulations, to have each caused increases of $\sim$ 1 million km$^2$ to the ozone hole area (Solomon et al., 2016). The Calbuco eruption (Chile, April 2015) has also been partly attributed as a cause of the large ozone hole in 2015 with a $\sim$ 4.5 million km$^2$ ($\sim$ 15%) area increase (Ivy et al., 2017). To further understand the impact of the Hunga eruption on ozone during the 2023 Antarctic spring, we also analyse the impact on the size of the Antarctic ozone hole for the ΔWater_Vapour experiment. Figure 8 puts the post-Hunga ozone holes (2022-2024) into the context of the record from when the ozone hole was beginning to emerge in 1979, grouping by decade (1979 - 1989, 1990 - 1999, 2000 - 2009, 2010 - 2019 (exclusive of 2015), 2020 - 2021) as both averages and individual years. The 2020 - 2021 lines (black) highlight the first of four anomalously large ozone holes (e.g. Wargan et al., 2025; Brühl et al., 2025), which were influenced by enhanced stratospheric aerosol loading from intense wildfires reaching the stratosphere (e.g Khaykin et al., 2020; Solomon et al., 2023), with 2022 and 2023 completing the set. The 2022 ozone hole (Fig.7, pink lines) did not show a chemical impact from the Hunga $H_2O$, the water vapour not having entered the vortex region at that time (Manney et al., 2023). Although there was no chemical impact from the Hunga $H_2O$, multi-model analysis shows the eruption still likely caused some additional ozone loss via dynamical effects, from an indirect vortex strengthening effect (Bednarz et al., 2025a, b). Furthermore, analysis in the Hunga report (Khaykin, Bourassa et al., 2025; Fig. 3.9) suggests a modest intrusion of volcanic aerosol did penetrate the 2022

https://doi.org/10.5194/egusphere-2026-3619
Preprint. Discussion started: 26 June 2026


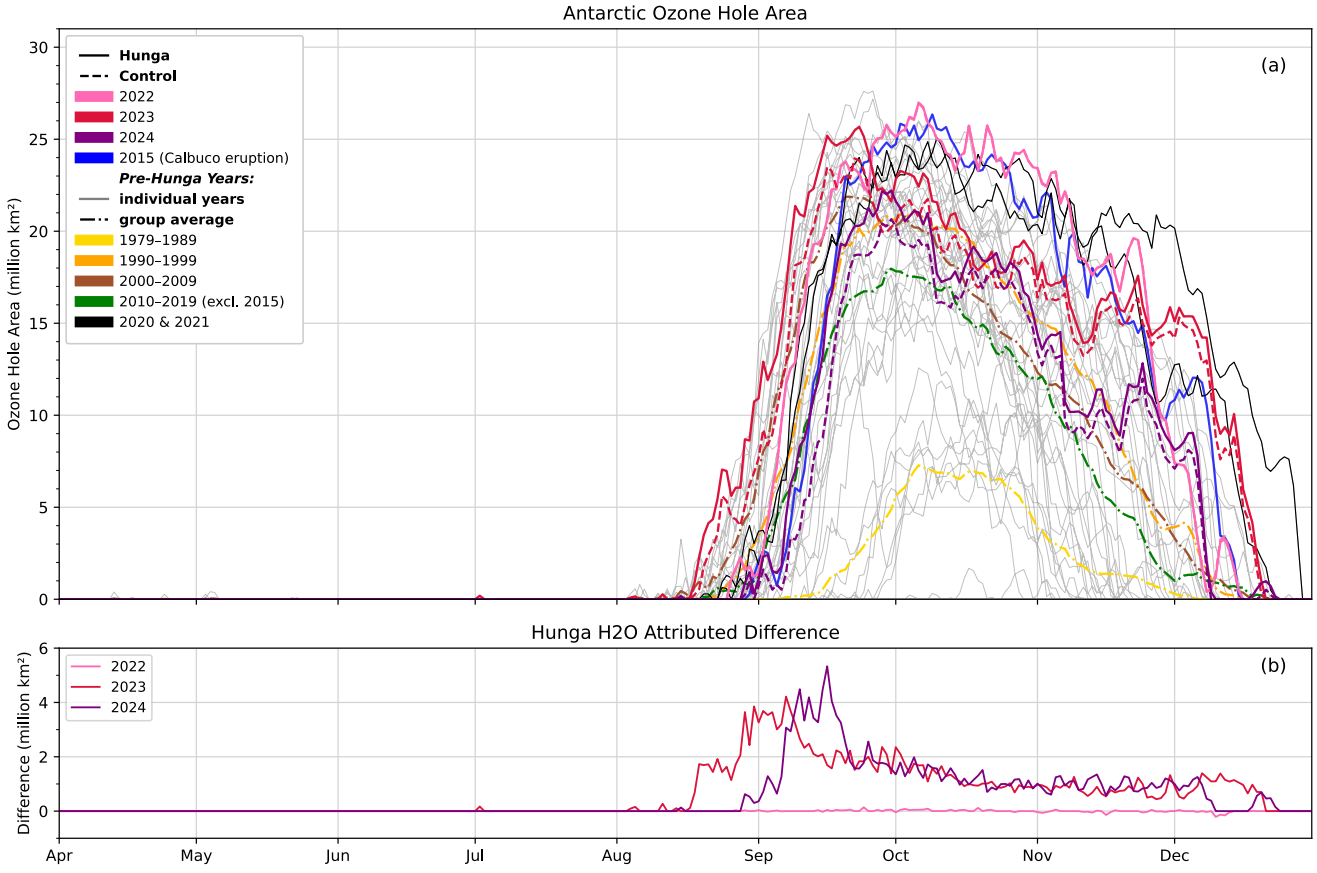


**Figure 8.** (a) Modelled Antarctic ozone hole area (million km$^2$) with the post-Hunga years 2022 (pink), 2023 (red), 2024 (purple), and Calbuco in 2015 (blue) highlighted. The highlighted years are placed into the context of the record from 1977 to 2021 from the Control_G simulation in grey with averages of the decades: 1979 - 1989 (yellow), 1990 - 1999 (orange), 2000 - 2009 (brown), and 2010 - 2019 (exclusive of 2015) (green). The first two, 2020 - 2021, of the period of four large ozone holes are highlighted in black. The ozone hole area is calculated using the 220 DU threshold. (b) Difference between the Hunga_H2O and Control_G ozone hole areas for the post-Hunga years to show the Hunga water-vapour-attributed impact.

Antarctic vortex, a weak layer of non-spherical backscatter seen in both ground-based and satellite lidar observations above Dumont D'Urville. The 2022 ozone hole had a larger peak area, similar to the 2020 and 2021 large ozone holes (Fig. 8, pink lines), and the anomaly compared to 2010-2019 is not inconsistent with a volcanic indirect effect (Bednarz et al., 2025b).

The 2023 Antarctic winter was the first to be directly, chemically impacted by the Hunga $H_2O$ and was the last of a period of anomalously large ozone holes. Figure 8 (red lines) shows the 2023 ozone hole began its formation unusually early from July into early August in both the Control_G and Hunga_H2O simulations with the area of the Hunga_H2O simulation increased by a maximum of 4.21 million km$^2$ (7th September 2023) relative to Control_G , the largest Hunga $H_2O$ induced chemical

https://doi.org/10.5194/egusphere-2026-3619
Preprint. Discussion started: 26 June 2026


increase of the 2023 season. The 2023 ozone hole then peaked in mid September to maximum areas of 23.96 million km$^2$ (22nd of September 2023) in Control_G and 25.68 million km$^2$ (23rd of September 2023) in Hunga_H2O , resulting in a 1.72 million km$^2$, 7.19%, difference between maximum areas. The magnitude of the difference decreased towards the end of the season and the ozone hole finished in mid-December as one of the longer lasting ozone holes in the record. Consequently resulting in an impressive, but not quite record-breaking ozone hole. The impact to the 2023 ozone hole appears quite modest, but we note that the the PSC dehydration removed the Hunga-excess $H_2O$ after day 70 of the April to December vortex period, meaning the core of the vortex was only enhanced for 25.55% of the vortex season.

The earlier start and later end of the ozone hole is present in both the Control_G and Hunga_H2O simulations, indicating the Hunga $H_2O$ is not the sole contributor to the impact on the ozone hole and there is likely to be influences from the sulfate aerosol and dynamics. Stratospheric temperature is one of the major factors controlling polar ozone depletion and can be influenced by changes in water vapour, aerosols, and ozone itself. Therefore it is important to consider, additional factors that might have influenced the stratospheric dynamics alongside the chemical impact of the $H_2O$. For the 2023 ozone hole Bednarz et al. (2025a) suggested although the chemical impact from the water vapour was still significant, the dynamical impact was likely to be as important and may have contributed around half of the impact to the additional ozone depletion. However, Chemistry Climate Models (CCMs) included in their study show large spread in model response in terms of the magnitude of the Antarctic ozone impact in 2023. The relative contribution of the dynamics vs the chemical impact also varied by altitude with the upper-stratosphere being largely chemically driven by the additional $H_2O$ accelerating the $HO_x$ catalysed ozone depletion, and the dynamical impact becoming as important as the chemical in the mid- and lower-stratosphere. Consequently, it is important to note this study uses a CTM, so can diagnose only the chemical impact. Both the Control_G and Hunga_H2O simulations are forced by the same ERA5 metrology, therefore they both include temperature and dynamical impacts from the eruption. But as is clear from the large size of 2022's ozone hole and the earlier start of the 2023 hole in both with and without the Hunga $H_2O$, the chemical impact linked to the water vapour is only a partial factor. Quantifying likely influences from dynamics, temperature, and the volcanic aerosol and the extent of these processes continue to remain as open research questions.

Figure 8 also includes 2024's ozone hole (purple lines) which was characterised by a warmer vortex with two consecutive sudden stratospheric warmings (SSWs) in July and August, a relatively rare occurrence in the Antarctic (Zi et al., 2025). Subsequently, the warmer vortex caused PSCs to be less prevalent so the usual limiting mechanisms did not restrict ozone loss in the vortex centre and there was less of a contrast between the edge and core regions. The 2024 Antarctic ozone hole started later than 2023 and had a smaller size but also showed a large impact from Hunga. The modelled difference in ozone hole area relative to the control in 2024 is, however, larger than 2023 in September and towards the end in mid-December (Fig. 8b, purple).

### 5.2 Sulfate aerosol contribution to the chemical impact to polar ozone in 2023

Large volcanic eruptions has been shown to cause additional polar ozone depletion from chlorine activation on the sulphate aerosol, for example after El Chichon (e.g. Hofmann and Solomon, 1989) and after Pinatubo (Hofmann and Oltmans, 1993). The model experiments listed in Table 2 cover the impact from the $H_2O$, stratospheric aerosol, and the combined impact.

https://doi.org/10.5194/egusphere-2026-3619
Preprint. Discussion started: 26 June 2026


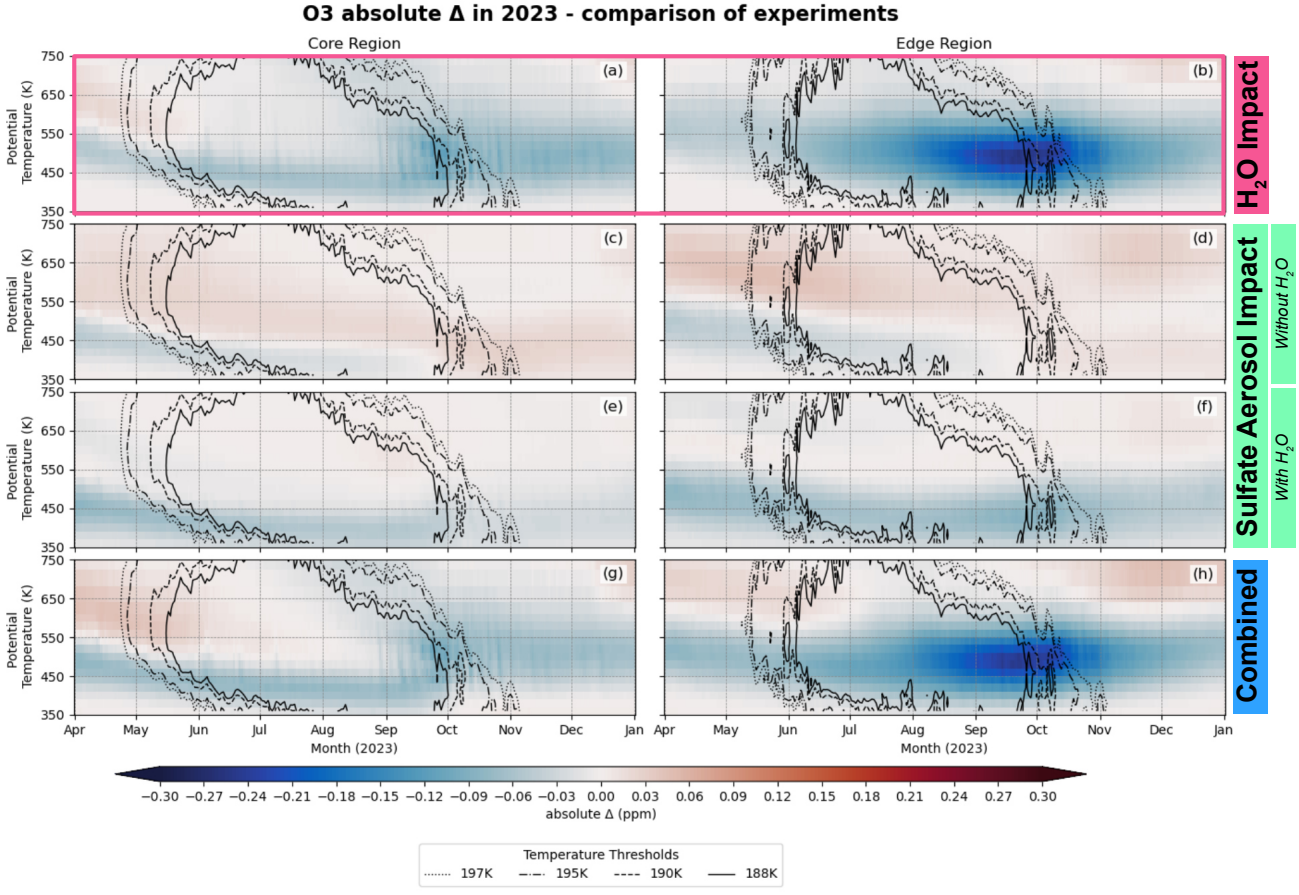


**Figure 9.** Ozone differences ($\Delta O_3$) in ppm from 1st April to December 31st 2023 for the model experiment combinations described in Table 2. The left column is for the core region (-90° to -70° EL) and right is the edge (-70° to -55° EL). All panels are overlaid with contours highlighting the PSC threshold temperatures for the NAT (195 K) and ice (188 K) in the minimum temperatures as solid lines. Dashed lines mark the threshold temperatures +2 K.

These experiments also show some regional differences between the core and edge regions as seen in ΔWater_Vapour (Fig. 9). Overall, the aerosol impact in ΔAerosol_noH2Ointeraction (without the interaction of the Hunga $H_2O$) show small increases in the mid-stratosphere ozone of 0.03 ppm in the core and 0.05 ppm in the edge regions (Fig. 9c-d). This increase in the core
485 starts above 550 K and descends over time maintaining a relatively constant magnitude. The edge shows a similar pattern but starting above 575 K. Both regions also show maximum additional ozone depletion of 0.05 ppm in April as a band that descends with positive values above and gradually diminishes towards October, without a peak when the sunlight returns.

In the experiment ΔAerosol_H2Ointeraction (where the Hunga $H_2O$ is interacting with the aerosol) the profile of the additional ozone depletion is very similar to ΔAerosol_noH2Ointeraction with 0.08 ppm in the core and 0.09 ppm in the edge (Fig.

https://doi.org/10.5194/egusphere-2026-3619
Preprint. Discussion started: 26 June 2026


9 e-f). However, ΔAerosol_H2Ointeraction does not show the positive ozone change seen in ΔAerosol_noH2Ointeraction , with a maximum of only 0.01 ppm additional ozone in both regions. The experiment ΔCombined (combined impact, with a 'clean' control) shows a similar profile and magnitude of change to the ΔWater_Vapour with distinct regional differences. The combined impact shows the greatest impact in the edge region with maximum additional ozone depletion of 0.25 ppm, compared to 0.11 ppm in the core. The main difference in the chemical ozone impact between the ΔWater_Vapour and ΔCombined experiments is the magnitude and vertical extent of the positive ozone change. The ΔCombined experiment shows, in both regions, maximum additional ozone of 0.05 ppm. However, the timings of the maximums are different between the two regions, with the core being in April and edge in November. Both regions show these positive values in a similar way to ΔAerosol_noH2Ointeraction , at the higher levels with the core >550 K and edge >650 K, both descending over time. However, unlike the ΔAerosol_noH2Ointeraction , the ΔCombined positive values diminish by July and are overtopped by negatives. It is possible the ozone increase in the middle stratosphere and the early season ozone changes are linked to changes in mid-latitude chemistry (Bednarz et al., 2025a). Therefore, the Hunga $H_2O$ was important in its interaction with the aerosol as well as the PSCs and the related chemistry. Consequently, Figure 9 shows the majority of the modelled chemical impact for the 2023 Antarctic ozone depletion appears to be predominantly driven by the $H_2O$. Relative to the maximum additional ozone depletion in the ΔCombined , the ΔWater_Vapour experiment impact was 9% and 4% larger for the core and the edge regions, respectively. The ΔAerosol_noH2Ointeraction was 54% (core) and 80% (edge) less and the ΔAerosol_H2Ointeraction was 27% (core) and 64% (edge) less. For the additional ozone (positive) relative to the ΔCombined the ΔWater_Vapour was 40% less for both regions, the ΔAerosol_noH2Ointeraction was 40% less for the core and the same as ΔCombined for the edge, and ΔAerosol_H2Ointeraction was 80% less for both regions. Therefore, overall for the chemical impact on Antarctic ozone in 2023, the Hunga aerosol reduced the additional springtime ozone depletion by a small amount.

Alongside volcanic eruptions another increasing concern to polar ozone, and therefore the ozone hole, is the increasing frequency of wildfires. Generally wildfire emissions stay within the troposphere, however exceptionally large wildfire events such as the Pacific North-West Event (PNE) and the Australian New Years (ANY) fires which generate pyrocumubnimbus (pyroCb) clouds and loft wildfire smoke into the lower stratosphere (Katich et al., 2023) are increasing in frequency due to climate change, and are only thought to increase further over the coming decades (Peterson et al., 2017; Di Virgilio et al., 2019). Extreme wildfire events with pyroCb clouds resulting in stratospheric impacts are thought to have comparable impacts to the aerosol from some large scale volcanic eruptions (Peterson et al., 2018). The impact of the ANY 2019-2020 wildfires on the 2020 ozone hole has been modelled to show a small increase of ozone depletion, resulting in a large area and record duration (Solomon et al., 2023). However, the 2020 ozone hole was the second of four large ozone holes between 2020 and 2023, and the influence of the ANY fires was not the sole cause of the larger ozone hole (Wargan et al., 2025). The modest influence of the ANY fires on the 2020 ozone hole was moderated by the higher solubility of HCl in (liquid) PSCs than organics at temperatures below 200 K. Therefore, further supporting the valuable role of PSCs in limiting the scale of the impact from large scale, stratospheric reaching, events such as extreme wildfires and volcanic eruptions on the ozone hole. However, it is important to also consider the role of temperature and dynamics alongside the chemical impact. Therefore, we must continue

https://doi.org/10.5194/egusphere-2026-3619
Preprint. Discussion started: 26 June 2026


to employ a wide range of models to support observations and understand the details of the impacts from previous and possible future events on the ozone hole.

## 6 Summary and conclusions

This study used 3-D global chemistry transport model (CTM) simulations and MLS observations to understand the driving processes behind the chemical impacts of the Hunga stratospheric $H_2O$ enhancement on the 2023 Antarctic ozone hole. We demonstrate how the impacts of Hunga on the Antarctic ozone hole were affected by the differing PSC regimes in the vortex edge region, compared to the much colder vortex core region. For this purpose, the model predicted chemical impacts from the Hunga $H_2O$ were analysed using an equivalent latitude co-ordinate system, with sensitivity simulations separately attributing the contributions from the $H_2O$, stratospheric aerosol, and their combined chemical impact. This study predominantly focused on the contribution of the $H_2O$ enhancement to the polar ozone chemistry.

The model simulations show that the longevity and the magnitude of the Hunga $H_2O$ impact was determined by the typical efficiency of processes related to PSCs such as dehydration (ice), denitrification (NAT), and chlorine processing through the heterogeneous chemistry. In both regions of the vortex, PSCs appeared earlier and generally with an increased areal extent due to the Hunga $H_2O$ enhancement. In the core region, temperatures regularly reach the ice threshold and the chlorine activation chemistry typically saturates or 'bottoms-out'. Hence, the impacts are reduced after dehydration which removed almost all the Hunga $H_2O$ enhancement in 2023, meaning the core was only enhanced for 25.55% of the April-December vortex season. In contrast, in the edge where the conditions are not as cold and ice PSCs do not occur as regularly, the response is larger. The dehydration via ice PSCs is less effective in the edge, resulting in $\sim$1 ppm of the $\sim$2.5 ppm enhancement remaining after an initial period of dehydration. In combination with the effective removal of the Hunga $H_2O$ enhancement, the typical efficiency of chlorine processing and denitrification in the core leads to large effects at the beginning of the season that are not maintained, resulting in an additional ozone loss of only 0.12 ppm in September 2023. In contrast, the heterogeneous chlorine processing and denitrification processes do not saturate in the vortex edge region so the earlier and increased area of PSCs means increased chlorine activation, more denitrification/renitrification, and greater ozone depletion reaching $-0.26$ ppm in September.

We therefore find that the impact from the Hunga $H_2O$ enhancement on chemical ozone depletion in the core was limited by three main factors: (1) the efficiency of the dehydration and denitrification via PSCs, (2) the saturation of the chlorine processing, and (3) the typically large ozone depletion in the core. This indicates that the very cold and efficient nature of the Antarctic vortex environment limited the impact of the Hunga $H_2O$ enhancement. It is possible the edge could be used to assess the impact of a Hunga-like eruption in a warmer winter and is potentially transferable to the Arctic. Together with Zhou et al. (2024) and Wohltmann et al. (2024) we show the critical importance of PSCs in controlling the timing, magnitude, and longevity of the impact from the Hunga $H_2O$ enhancement in the cold Antarctic vortex.

Importantly, the increased ozone depletion across the vortex resulted in an increased maximum ozone hole area of 1.72 million $km^2$ (7 %), relative to a control simulation, in 2023. This increased an already large ozone hole in a period of large

https://doi.org/10.5194/egusphere-2026-3619
Preprint. Discussion started: 26 June 2026


holes between 2020 and 2023, but remaining within the historical interannual variability. It should be noted, as this study uses a CTM, we do not directly analyse the effects on temperature or dynamics, both of which will influence the development of the ozone hole.

Finally, through a series of sensitivity studies we show the main driver of the additional springtime chemical ozone loss was mostly linked to the $H_2O$ enhancement with the volcanic sulfate aerosol reducing the impact of the $H_2O$ on polar ozone by 4% in the edge and 9% in the core relative to the combined impact. Much of the overall contribution from the sulfate aerosol is likely from chemical processes occurring in the mid-latitudes which is then transported to the polar region (Bednarz et al., 2025a).

This study used a CTM with all simulations forced using the same ERA5/5.1 dataset. Thus we are not able to quantify any dynamical or radiative impacts directly. However, by using the CTM we have been able to effectively isolate the chemical mechanisms of the impact to the Antarctic ozone depletion in 2023 using realistic meteorology.

*Data availability.* NASA Aura Microwave limb sounder vertical profiles (level 2) of $O_3$, HCl, $H_2O$, $HNO_3$, and ClO, and daily binned level 3 (ML3DB) are obtained via https://search.earthdata.nasa.gov/. TOMCAT model simulations will be made available after acceptance of this paper.

*Author contributions.* SGH and GWM led the initial experiment design, model simulations, data analysis, and the writing of the paper. MPC and SSD contributed to the initial experiment design and model simulations. SGH led the data analysis and the writing with guidance from GWM, MPC, and SSD. SGH, WF, MY, and MPC contributed to the core/edge definitions using the equivalent latitude method. All authors contributed to the final stages of the writing.

*Competing interests.* The authors declare no competing interests.

*Acknowledgements.* SGH is funded by the Leeds-York-Hull Natural Environment Research Council (NERC) Doctoral Training Partnership (DTP) Panorama under grant NE/S007458/1. SGH also receives funding and support from the UK Met Office through a CASE partnership. MPC and SSD acknowledge the funding from NERC grants NE/V011863/1 and NE/X003450/1. GWM and MY acknowledge funding from NERC standard grant project MeteorStrat (grant no. NE/R011222/1). GWM and SSD acknowledge funding from the UK National Centre for Atmospheric Science (NCAS) via the NERC multi-centre Long-Term Science programme on the North Atlantic climate system (ACSIS, NERC grant NE/N018001/1). XZ acknowledges funding from the National Natural Science Foundation of China (U2442210, 42275059, 12411530093). MY acknowledges funding from the NERC MAGICA grant (NE/Z503836/1). SGH also acknowledges the support from the University of Leeds TOMCAT research group, Aerosols, Clouds & climate group, and peers, particularly Alicia Hoffman and Maria Paula Velásquez García for computational and insightful discussions throughout the course of this work.

https://doi.org/10.5194/egusphere-2026-3619
Preprint. Discussion started: 26 June 2026


This work used ARC4, part of the High Performance Computing facilities at the University of Leeds, UK and the ARCHER2 UK National Supercomputing Service (https://www.archer2.ac.uk).

https://doi.org/10.5194/egusphere-2026-3619
Preprint. Discussion started: 26 June 2026


## References

Alfred, J., Fromm, M., Bevilacqua, R., Nedoluha, G., Strawa, A., Poole, L., and Wickert, J.: Observations and analysis of polar stratospheric clouds detected by POAM III and SAGE III during the SOLVE II/VINTERSOL campaign in the 2002/2003 Northern Hemisphere winter, Atmos. Chem. Phys., 2007.

APARC: The Hunga Volcanic Eruption Atmospheric Impacts Report, edited by Yunqian Zhu, Graham Mann, Paul A. Newman, and William Randel. APARC Report No. 11, WCRP Report No. 10/2025, https://doi.org/10.2172/3012479, 2025.

Arfeuille, F., Weisenstein, D., Mack, H., Rozanov, E., Peter, T., and Brönnimann, S.: Volcanic forcing for climate modeling: a new microphysics-based data set covering years 1600–present, Climate of the Past, 10, 359–375, https://doi.org/10.5194/cp-10-359-2014, 2014.

Bednarz, E. M., Aquila, V., Butler, A. H., Colarco, P., Fleming, E., Østerstrøm, F. F., Plummer, D., Quaglia, I., Randel, W., Santee, M. L., Sekiya, T., Tilmes, S., Wang, X., Watanabe, S., Yu, W., Zhang, J., Zhu, Y., and Zhuo, Z.: Multi-model assessment of impacts of the 2022 Hunga eruption on stratospheric ozone and its chemical and dynamical drivers, https://doi.org/10.5194/egusphere-2025-4609, 2025a.

Bednarz, E. M., Butler, A. H., Wang, X., Zhuo, Z., Yu, W., Stenchikov, G., Toohey, M., and Zhu, Y.: Indirect climate impacts of the Hunga eruption, https://doi.org/10.5194/egusphere-2025-1970, 2025b.

Brühl, C., Kohl, M., Lelieveld, J., Rieger, L., and Santee, M.: Radiative forcing and stratospheric ozone changes due to major forest fires and recent volcanic eruptions including Hunga Tonga, https://doi.org/10.5194/egusphere-egu25-3642, 2025.

Carn, S., Schmidt, A., et al.: Volcanological context of the 2022 Hunga eruption, in APARC, 2025: The Hunga Eruption Atmospheric Impacts Report [Yunqian Zhu, Graham Mann, Paul A. Newman, William Randel (Eds.)]. APARC Report No. 11, WCRP Report No. 10/2025, https://doi.org/10.34734/FZJ-2025-05238, 2025.

Carn, S. A., Krotkov, N. A., Fisher, B. L., and Li, C.: Out of the blue: Volcanic SO2 emissions during the 2021–2022 eruptions of Hunga Tonga—Hunga Ha'apai (Tonga), Frontiers in Earth Science, 10, 976 962, https://doi.org/10.3389/feart.2022.976962, 2022.

Carslaw, K. S., Luo, B., and Peter, T.: An analytic expression for the composition of aqueous $HNO_3$ -$H_2$ $SO_4$ stratospheric aerosols including gas phase removal of $HNO_3$, Geophysical Research Letters, 22, 1877–1880, https://doi.org/10.1029/95GL01668, 1995.

Chipperfield, M. P.: New version of the TOMCAT/SLIMCAT off-line chemical transport model: Intercomparison of stratospheric tracer experiments, Quarterly Journal of the Royal Meteorological Society, 132, 1179–1203, https://doi.org/10.1256/qj.05.51, 2006.

Chipperfield, M. P.: Ongoing large ozone depletion in the polar lower stratospheres: the role of increased water vapour, Faraday Discuss., 2025.

Chipperfield, M. P., Cariolle, D., Simon, P., Ramaroson, R., and Lary, D. J.: A three-dimensional modeling study of trace species in the Arctic lower stratosphere during winter 1989–1990, Journal of Geophysical Research: Atmospheres, 98, 7199–7218, https://doi.org/10.1029/92JD02977, 1993.

Chipperfield, M. P., Santee, M. L., Froidevaux, L., Manney, G. L., Read, W. G., Waters, J. W., Roche, A. E., and Russell, J. M.: Analysis of UARS data in the southern polar vortex in September 1992 using a chemical transport model, Journal of Geophysical Research: Atmospheres, 101, 18 861–18 881, https://doi.org/10.1029/96JD00936, 1996.

Clyne, M., Toon, O. B., Sukhodolov, T., Mann, G. W., Dhomse, S., Tilmes, S., Zhu, Y., Colarco, P. R., Tsigaridis, K., and Nagashima, T.: Tonga-MIP: The Hunga Tonga-Hunga Ha'apai Volcano Model Intercomparison Project, in: Modeling the Role of Volcanoes in the Climate System (Publication No. 31487034), PhD thesis. University of Colorado Boulder, https://www.proquest.com/dissertations-theses/modeling-role-volcanoes-climate-system/docview/3100397790/se-2., 2024.

https://doi.org/10.5194/egusphere-2026-3619
Preprint. Discussion started: 26 June 2026


Coddington, O., Lean, J., Pilewskie, P., Snow, M., Richard, E., Kopp, G., Lindholm, C., DeLand, M., Marchenko, S., Haberreiter, M., and Baranyi, T.: Solar Irradiance Variability: Comparisons of Models and Measurements, Earth and Space Science, 6, 2525–2555, https://doi.org/10.1029/2019EA000693, 2019.

Crutzen, P. J. and Arnoldt, F.: Nitric acid cloud formation in the cold Antarctic stratosphere: a major cause for the springtime 'ozone hole', 1986.

Damany-Pearce, L., Johnson, B., Wells, A., Osborne, M., Allan, J., Belcher, C., Jones, A., and Haywood, J.: Australian wildfires cause the largest stratospheric warming since Pinatubo and extends the lifetime of the Antarctic ozone hole, Scientific Reports, 12, 12 665, https://doi.org/10.1038/s41598-022-15794-3, 2022.

Davies, d. S.: Denitrification and ozone loss in the Arctic stratosphere, Ph.D. thesis, University of Leeds, https://etheses.whiterose.ac.uk/id/eprint/6554/, 2003.

Davies, S., Chipperfield, M. P., Carslaw, K. S., Sinnhuber, B., Anderson, J. G., Stimpfle, R. M., Wilmouth, D. M., Fahey, D. W., Popp, P. J., Richard, E. C., Von Der Gathen, P., Jost, H., and Webster, C. R.: Modeling the effect of denitrification on Arctic ozone depletion during winter 1999/2000, Journal of Geophysical Research: Atmospheres, 107, https://doi.org/10.1029/2001JD000445, 2002.

Dhomse, S. S., Chipperfield, M. P., Feng, W., Hossaini, R., Mann, G. W., and Santee, M. L.: Revisiting the hemispheric asymmetry in midlatitude ozone changes following the Mount Pinatubo eruption: A 3-D model study, Geophysical Research Letters, 42, 3038–3047, https://doi.org/10.1002/2015GL063052, 2015.

Dhomse, S. S., Chipperfield, M. P., Damadeo, R. P., Zawodny, J. M., Ball, W. T., Feng, W., Hossaini, R., Mann, G. W., and Haigh, J. D.: On the ambiguous nature of the 11 year solar cycle signal in upper stratospheric ozone, Geophysical Research Letters, 43, 7241–7249, https://doi.org/10.1002/2016GL069958, 2016.

Dhomse, S. S., Mann, G. W., Antuña Marrero, J. C., Shallcross, S. E., Chipperfield, M. P., Carslaw, K. S., Marshall, L., Abraham, N. L., and Johnson, C. E.: Evaluating the simulated radiative forcings, aerosol properties, and stratospheric warmings from the 1963 Mt Agung, 1982 El Chichón, and 1991 Mt Pinatubo volcanic aerosol clouds, Atmospheric Chemistry and Physics, 20, 13 627–13 654, https://doi.org/10.5194/acp-20-13627-2020, 2020.

Di Virgilio, G., Evans, J. P., Blake, S. A. P., Armstrong, M., Dowdy, A. J., Sharples, J., and McRae, R.: Climate Change Increases the Potential for Extreme Wildfires, Geophysical Research Letters, 46, 8517–8526, https://doi.org/10.1029/2019GL083699, 2019.

Drdla, K., Gandrud, B. W., Baumgardner, D., Wilson, J. C., Bui, T. P., Hurst, D., Schauffler, S. M., Jost, H., Greenblatt, J. B., and Webster, C. R.: Evidence for the widespread presence of liquid-phase particles during the 1999–2000 Arctic winter, Journal of Geophysical Research: Atmospheres, 107, https://doi.org/10.1029/2001JD001127, 2002.

Dyer, A. J.: The effect of volcanic eruptions on global turbidity, and an attempt to detect long-term trends due to man, Quarterly Journal of the Royal Meteorological Society, 100, 563–571, https://doi.org/10.1002/qj.49710042606, 1974.

Fahey, D. W., Gao, R. S., Carslaw, K. S., Kettleborough, J., Popp, P. J., Northway, M. J., Holecek, J. C., Ciciora, S. C., McLaughlin, R. J., Thompson, T. L., Winkler, R. H., Baumgardner, D. G., Gandrud, B., Wennberg, P. O., Dhaniyala, S., McKinney, K., Peter, T., Salawitch, R. J., Bui, T. P., Elkins, J. W., Webster, C. R., Atlas, E. L., Jost, H., Wilson, J. C., Herman, R. L., Kleinböhl, A., and Von König, M.: The Detection of Large $HNO_3$ -Containing Particles in the Winter Arctic Stratosphere, Science, 291, 1026–1031, https://doi.org/10.1126/science.1057265, 2001.

Feng, W., Chipperfield, M. P., Davies, S., Mann, G. W., Carslaw, K. S., Dhomse, S., Harvey, L., Randall, C., and Santee, M. L.: Modelling the effect of denitrification on polar ozone depletion for Arctic winter 2004/2005, Atmospheric Chemistry and Physics, 11, 6559–6573, https://doi.org/10.5194/acp-11-6559-2011, 2011.

https://doi.org/10.5194/egusphere-2026-3619
Preprint. Discussion started: 26 June 2026


Fleming, E. L., Newman, P. A., Liang, Q., and Oman, L. D.: Stratospheric Temperature and Ozone Impacts of the Hunga Tonga-Hunga Ha'apai Water Vapor Injection, Journal of Geophysical Research: Atmospheres, 129, e2023JD039 298, https://doi.org/10.1029/2023JD039298, 2024.

Hall, T. M. and Waugh, D. W.: Timescales for the stratospheric circulation derived from tracers, Journal of Geophysical Research: Atmospheres, 102, 8991–9001, https://doi.org/10.1029/96JD03713, 1997.

Hanson, D. and Mauersberger, K.: Laboratory studies of the nitric acid trihydrate: Implications for the south polar stratosphere, Geophysical Research Letters, 15, 855–858, https://doi.org/10.1029/GL015i008p00855, 1988.

Harvey, V. L., Randall, C. E., and Hitchman, M. H.: Breakdown of potential vorticity–based equivalent latitude as a vortex-centered coordinate in the polar winter mesosphere, Journal of Geophysical Research: Atmospheres, 114, 2009JD012 681, https://doi.org/10.1029/2009JD012681, 2009.

Hersbach, H., Bell, B., Berrisford, P., Hirahara, S., Horányi, A., Muñoz-Sabater, J., Nicolas, J., Peubey, C., Radu, R., Schepers, D., Simmons, A., Soci, C., Abdalla, S., Abellan, X., Balsamo, G., Bechtold, P., Biavati, G., Bidlot, J., Bonavita, M., De Chiara, G., Dahlgren, P., Dee, D., Diamantakis, M., Dragani, R., Flemming, J., Forbes, R., Fuentes, M., Geer, A., Haimberger, L., Healy, S., Hogan, R. J., Hólm, E., Janisková, M., Keeley, S., Laloyaux, P., Lopez, P., Lupu, C., Radnoti, G., De Rosnay, P., Rozum, I., Vamborg, F., Villaume, S., and Thépaut, J.: The ERA5 global reanalysis, Quarterly Journal of the Royal Meteorological Society, 146, 1999–2049, https://doi.org/10.1002/qj.3803, 2020.

Hofmann, D. J. and Oltmans, S. J.: Anomalous Antarctic ozone during 1992: Evidence for Pinatubo volcanic aerosol effects, Journal of Geophysical Research: Atmospheres, 98, 18 555–18 561, https://doi.org/10.1029/93JD02092, 1993.

Hofmann, D. J. and Solomon, S.: Ozone destruction through heterogeneous chemistry following the eruption of El Chichón, Journal of Geophysical Research: Atmospheres, 94, 5029–5041, https://doi.org/10.1029/JD094iD04p05029, 1989.

James, A. D., Brooke, J. S. A., Mangan, T. P., Whale, T. F., Plane, J. M. C., and Murray, B. J.: Nucleation of nitric acid hydrates in polar stratospheric clouds by meteoric material, Atmospheric Chemistry and Physics, 18, 4519–4531, https://doi.org/10.5194/acp-18-4519-2018, 2018.

James, A. D., Pace, F., Sikora, S. N. F., Mann, G. W., Plane, J. M. C., and Murray, B. J.: The importance of acid-processed meteoric smoke relative to meteoric fragments for crystal nucleation in polar stratospheric clouds, Atmospheric Chemistry and Physics, 23, 2215–2233, https://doi.org/10.5194/acp-23-2215-2023, 2023.

Jensen, E. J., Toon, O. B., Tabazadeh, A., and Drdla, K.: Impact of polar stratospheric cloud particle composition, number density, and lifetime on denitrification, Journal of Geophysical Research: Atmospheres, 107, https://doi.org/10.1029/2001JD000440, 2002.

Joshi, M. M. and Jones, G. S.: The climatic effects of the direct injection of water vapour into the stratosphere by large volcanic eruptions, Atmos. Chem. Phys., 2009.

Katich, J. M., Apel, E. C., Bourgeois, I., Brock, C. A., Bui, T. P., Campuzano-Jost, P., Commane, R., Daube, B., Dollner, M., Fromm, M., Froyd, K. D., Hills, A. J., Hornbrook, R. S., Jimenez, J. L., Kupc, A., Lamb, K. D., McKain, K., Moore, F., Murphy, D. M., Nault, B. A., Peischl, J., Perring, A. E., Peterson, D. A., Ray, E. A., Rosenlof, K. H., Ryerson, T., Schill, G. P., Schroder, J. C., Weinzierl, B., Thompson, C., Williamson, C. J., Wofsy, S. C., Yu, P., and Schwarz, J. P.: Pyrocumulonimbus affect average stratospheric aerosol composition, Science, 379, 815–820, https://doi.org/10.1126/science.add3101, 2023.

Khaykin, S., Legras, B., Bucci, S., Sellitto, P., Isaksen, L., Tencé, F., Bekki, S., Bourassa, A., Rieger, L., Zawada, D., Jumelet, J., and Godin-Beekmann, S.: The 2019/20 Australian wildfires generated a persistent smoke-charged vortex rising up to 35 km altitude, Communications Earth & Environment, 1, 22, https://doi.org/10.1038/s43247-020-00022-5, 2020.

https://doi.org/10.5194/egusphere-2026-3619
Preprint. Discussion started: 26 June 2026


Khaykin, S., Bourassa, A., et al.: Atmospheric transport and evolution of Hunga water vapour and aerosols, in APARC, 2025: The Hunga Eruption Atmospheric Impacts Report [Yunqian Zhu, Graham Mann, Paul A. Newman, William Randel (Eds.)]. APARC Report No. 11, WCRP Report No. 10/2025, https://doi.org/10.34734/FZJ-2025-05240, 2025.

Khosrawi, F., Urban, J., Lossow, S., Stiller, G., Weigel, K., Braesicke, P., Pitts, M. C., Rozanov, A., Burrows, J. P., and Murtagh, D.: Sensitivity of polar stratospheric cloud formation to changes in water vapour and temperature, Atmospheric Chemistry and Physics, 16, 101–121, https://doi.org/10.5194/acp-16-101-2016, 2016.

Knepp, T. N., Kovilakam, M., Thomason, L., and Miller, S. J.: Characterization of stratospheric particle size distribution uncertainties using SAGE II and SAGE III/ISS extinction spectra, Atmospheric Measurement Techniques, 17, 2025–2054, https://doi.org/10.5194/amt-17-2025-2024, 2024.

Kremser, S., Thomason, L. W., von Hobe, M., Hermann, M., Deshler, T., Timmreck, C., Toohey, M., Stenke, A., Schwarz, J. P., Weigel, R., Fueglistaler, S., Prata, F. J., Vernier, J. P., Schlager, H., Barnes, J. E., Antuña-Marrero, J. C., Fairlie, D., Palm, M., Mahieu, E., Notholt, J., Rex, M., Bingen, C., Vanhellemont, F., Bourassa, A., Plane, J. M., Klocke, D., Carn, S. A., Clarisse, L., Trickl, T., Neely, R., James, A. D., Rieger, L., Wilson, J. C., and Meland, B.: Stratospheric aerosol—Observations, processes, and impact on climate, Reviews of Geophysics, 54, 278–335, https://doi.org/10.1002/2015RG000511, 2016.

Kuttippurath, J., Feng, W., Müller, R., Kumar, P., Raj, S., Gopikrishnan, G. P., and Roy, R.: Exceptional loss in ozone in the Arctic winter/spring of 2019/2020, Atmospheric Chemistry and Physics, 21, 14 019–14 037, https://doi.org/10.5194/acp-21-14019-2021, 2021.

Lait, L. R.: An Alternative Form for Potential Vorticity, Journal of the Atmospheric Sciences, 51, 1754–1759, https://doi.org/10.1175/1520-0469(1994)051<1754:AAFFPV>2.0.CO;2, 1994.

Lee, A. M., Roscoe, H. K., Jones, A. E., Haynes, P. H., Shuckburgh, E. F., Morrey, M. W., and Pumphrey, H. C.: The impact of the mixing properties within the Antarctic stratospheric vortex on ozone loss in spring, Journal of Geophysical Research: Atmospheres, 106, 3203–3211, https://doi.org/10.1029/2000JD900398, 2001.

Legras, B., Duchamp, C., Sellitto, P., Podglajen, A., Carboni, E., Siddans, R., Grooß, J.-U., Khaykin, S., and Ploeger, F.: The evolution and dynamics of the Hunga Tonga–Hunga Ha'apai sulfate aerosol plume in the stratosphere, Atmospheric Chemistry and Physics, 22, 14 957–14 970, https://doi.org/10.5194/acp-22-14957-2022, 2022.

Manney, G. L., Santee, M. L., Lambert, A., Millán, L. F., Minschwaner, K., Werner, F., Lawrence, Z. D., Read, W. G., Livesey, N. J., and Wang, T.: Siege in the Southern Stratosphere: Hunga Tonga-Hunga Ha'apai Water Vapor Excluded From the 2022 Antarctic Polar Vortex, Geophysical Research Letters, 50, e2023GL103 855, https://doi.org/10.1029/2023GL103855, 2023.

Marti, J. and Mauersberger, K.: A survey and new measurements of ice vapor pressure at temperatures between 170 and 250K, Geophysical Research Letters, 20, 363–366, https://doi.org/10.1029/93GL00105, 1993.

Millán, L., Santee, M. L., Lambert, A., Livesey, N. J., Werner, F., Schwartz, M. J., Pumphrey, H. C., Manney, G. L., Wang, Y., Su, H., Wu, L., Read, W. G., and Froidevaux, L.: The Hunga Tonga-Hunga Ha'apai Hydration of the Stratosphere, Geophysical Research Letters, 49, e2022GL099 381, https://doi.org/10.1029/2022GL099381, 2022.

Molina, M. J., Zhang, R., Wooldridge, P. J., McMahon, J. R., Kim, J. E., Chang, H. Y., and Beyer, K. D.: Physical Chemistry of the $H_2$ $SO_4$ /$HNO_3$ /$H_2$ O System: Implications for Polar Stratospheric Clouds, Science, 261, 1418–1423, https://doi.org/10.1126/science.261.5127.1418, 1993.

Nash, E. R., Newman, P. A., Rosenfield, J. E., and Schoeberl, M. R.: An objective determination of the polar vortex using Ertel's potential vorticity, Journal of Geophysical Research: Atmospheres, 101, 9471–9478, https://doi.org/10.1029/96JD00066, 1996.

https://doi.org/10.5194/egusphere-2026-3619
Preprint. Discussion started: 26 June 2026


Newhall, C. G. and Self, S.: The volcanic explosivity index (VEI) an estimate of explosive magnitude for historical volcanism, Journal of Geophysical Research: Oceans, 87, 1231–1238, https://doi.org/10.1029/JC087iC02p01231, 1982.

Peterson, D. A., Fromm, M. D., Solbrig, J. E., Hyer, E. J., Surratt, M. L., and Campbell, J. R.: Detection and Inventory of Intense Pyroconvection in Western North America using GOES-15 Daytime Infrared Data, Journal of Applied Meteorology and Climatology, 56, 471–493, https://doi.org/10.1175/JAMC-D-16-0226.1, 2017.

Peterson, D. A., Campbell, J. R., Hyer, E. J., Fromm, M. D., Kablick, G. P., Cossuth, J. H., and DeLand, M. T.: Wildfire-driven thunderstorms cause a volcano-like stratospheric injection of smoke, npj Climate and Atmospheric Science, 1, 30, https://doi.org/10.1038/s41612-018-0039-3, 2018.

Poli, P. and Shapiro, N. M.: Rapid Characterization of Large Volcanic Eruptions: Measuring the Impulse of the Hunga Tonga Ha'apai Explosion From Teleseismic Waves, Geophysical Research Letters, 49, e2022GL098 123, https://doi.org/10.1029/2022GL098123, 2022.

Proud, S. R., Prata, A. T., and Schmauß, S.: The January 2022 eruption of Hunga Tonga-Hunga Ha'apai volcano reached the mesosphere, Science, 378, 554–557, https://doi.org/10.1126/science.abo4076, 2022.

Robock, A.: Volcanic eruptions and climate, Reviews of Geophysics, 38, 191–219, https://doi.org/10.1029/1998RG000054, 2000.

Roscoe, H. K., Feng, W., Chipperfield, M. P., Trainic, M., and Shuckburgh, E. F.: The existence of the edge region of the Antarctic stratospheric vortex, Journal of Geophysical Research: Atmospheres, 117, 2011JD015 940, https://doi.org/10.1029/2011JD015940, 2012.

Santee, M. L., Manney, G. L., Lambert, A., Millán, L. F., Livesey, N. J., Pitts, M. C., Froidevaux, L., Read, W. G., and Fuller, R. A.: The Influence of Stratospheric Hydration From the Hunga Eruption on Chemical Processing in the 2023 Antarctic Vortex, Journal of Geophysical Research: Atmospheres, 129, e2023JD040 687, https://doi.org/10.1029/2023JD040687, 2024.

Seinfeld, J. and Pandis, S.: Atmospheric chemistry and physics: from air pollution to climate change, John Wiley & Sons, Inc., Hoboken, New Jersey, third edn., 2016.

Sellitto, P., Podglajen, A., Belhadji, R., Boichu, M., Carboni, E., Cuesta, J., Duchamp, C., Kloss, C., Siddans, R., Bègue, N., Blarel, L., Jegou, F., Khaykin, S., Renard, J. B., and Legras, B.: The unexpected radiative impact of the Hunga Tonga eruption of 15th January 2022, Communications Earth & Environment, 3, 288, https://doi.org/10.1038/s43247-022-00618-z, 2022.

Solomon, S.: The mystery of the Antarctic Ozone "Hole", Reviews of Geophysics, 26, 131–148, https://doi.org/10.1029/RG026i001p00131, 1988.

Solomon, S.: Stratospheric ozone depletion: A review of concepts and history, Reviews of Geophysics, 37, 275–316, https://doi.org/10.1029/1999RG900008, 1999.

Solomon, S., Garciat, R. R., Rowland, F. S., and Wuebbles, D. J.: On the depletion of Antarctic ozone, 1986.

Solomon, S., Ivy, D. J., Kinnison, D., Mills, M. J., Neely, R. R., and Schmidt, A.: Emergence of healing in the Antarctic ozone layer, Science, 353, 269–274, https://doi.org/10.1126/science.aae0061, 2016.

Solomon, S., Stone, K., Yu, P., Murphy, D. M., Kinnison, D., Ravishankara, A. R., and Wang, P.: Chlorine activation and enhanced ozone depletion induced by wildfire aerosol, Nature, 615, 259–264, https://doi.org/10.1038/s41586-022-05683-0, 2023.

Thomason, L. W., Poole, L. R., and Deshler, T.: A global climatology of stratospheric aerosol surface area density deduced from Stratospheric Aerosol and Gas Experiment II measurements: 1984–1994, Journal of Geophysical Research: Atmospheres, 102, 8967–8976, https://doi.org/10.1029/96JD02962, 1997.

Toohey, M., Krüger, K., Niemeier, U., and Timmreck, C.: The influence of eruption season on the global aerosol evolution and radiative impact of tropical volcanic eruptions, Atmospheric Chemistry and Physics, 11, 12 351–12 367, https://doi.org/10.5194/acp-11-12351-2011, 2011.

https://doi.org/10.5194/egusphere-2026-3619
Preprint. Discussion started: 26 June 2026


Toohey, M., Jia, Y., Khanal, S., and Tegtmeier, S.: Stratospheric residence time and the lifetime of volcanic stratospheric aerosols, Atmospheric Chemistry and Physics, 25, 3821–3839, https://doi.org/10.5194/acp-25-3821-2025, 2025.

Toon, O. B., Hamill, P., Turco, R. P., and Pinto, J.: Condensation of $HNO_3$ and HCl in the winter polar stratospheres, Geophysical Research Letters, 13, 1284–1287, https://doi.org/10.1029/GL013i012p01284, 1986.

Tritscher, I., Pitts, M. C., Poole, L. R., Alexander, S. P., Cairo, F., Chipperfield, M. P., Grooß, J. U., Höpfner, M., Lambert, A., Luo, B., Molleker, S., Orr, A., Salawitch, R., Snels, M., Spang, R., Woiwode, W., and Peter, T.: Polar Stratospheric Clouds: Satellite Observations, Processes, and Role in Ozone Depletion, Reviews of Geophysics, 59, https://doi.org/10.1029/2020RG000702, 2021.

Vömel, H., Evan, S., and Tully, M.: Water vapor injection into the stratosphere by Hunga Tonga-Hunga Ha'apai, Science, 377, 1444–1447, https://doi.org/10.1126/science.abq2299, 2022.

Wang, X., Randel, W., Zhu, Y., Tilmes, S., Starr, J., Yu, W., Garcia, R., Toon, O. B., Park, M., Kinnison, D., Zhang, J., Bourassa, A., Rieger, L., Warnock, T., and Li, J.: Stratospheric Climate Anomalies and Ozone Loss Caused by the Hunga Tonga-Hunga Ha'apai Volcanic Eruption, Journal of Geophysical Research: Atmospheres, 128, e2023JD039 480, https://doi.org/10.1029/2023JD039480, 2023.

Wang, X., Coy, L., et al.: Hunga effects on stratospheric temperatures and circulation, in APARC, 2025: The Hunga Eruption Atmospheric Impacts Report [Yunqian Zhu, Graham Mann, Paul A. Newman, William Randel (Eds.)]. APARC Report No. 11, WCRP Report No. 10/2025, https://doi.org/10.34734/FZJ-2025-05241, 2025.

Wargan, K., Manney, G. L., and Livesey, N. J.: Factors contributing to the unusually low Antarctic springtime ozone in 2020-2023, https://doi.org/10.22541/essoar.173940272.21623654/v1, 2025.

Waters, J., Froidevaux, L., Harwood, R., Jarnot, R., Pickett, H., Read, W., Siegel, P., Cofield, R., Filipiak, M., Flower, D., Holden, J., Lau, G., Livesey, N., Manney, G., Pumphrey, H., Santee, M., Wu, D., Cuddy, D., Lay, R., Loo, M., Perun, V., Schwartz, M., Stek, P., Thurstans, R., Boyles, M., Chandra, K., Chavez, M., Gun-Shing Chen, Chudasama, B., Dodge, R., Fuller, R., Girard, M., Jiang, J., Yibo Jiang, Knosp, B., LaBelle, R., Lam, J., Lee, K., Miller, D., Oswald, J., Patel, N., Pukala, D., Quintero, O., Scaff, D., Van Snyder, W., Tope, M., Wagner, P., and Walch, M.: The Earth observing system microwave limb sounder (EOS MLS) on the aura Satellite, IEEE Transactions on Geoscience and Remote Sensing, 44, 1075–1092, https://doi.org/10.1109/TGRS.2006.873771, 2006.

Wilmouth, D. M., Stimpfle, R. M., Anderson, J. G., Elkins, J. W., Hurst, D. F., Salawitch, R. J., and Lait, L. R.: Evolution of inorganic chlorine partitioning in the Arctic polar vortex, Journal of Geophysical Research: Atmospheres, 111, 2005JD006 951, https://doi.org/10.1029/2005JD006951, 2006.

Wilmouth, D. M., Østerstrøm, F. F., Smith, J. B., Anderson, J. G., and Salawitch, R. J.: Impact of the Hunga Tonga volcanic eruption on stratospheric composition, Proceedings of the National Academy of Sciences, 120, e2301994 120, https://doi.org/10.1073/pnas.2301994120, 2023.

Wohltmann, I., Santee, M. L., Manney, G. L., and Millán, L. F.: The Chemical Effect of Increased Water Vapor From the Hunga Tonga-Hunga Ha'apai Eruption on the Antarctic Ozone Hole, Geophysical Research Letters, 51, e2023GL106 980, https://doi.org/10.1029/2023GL106980, 2024.

World Meteorological Organization (WMO).: Scientific Assessment of Ozone Depletion: 2022, Tech. Rep. 278, Geneva, Switzerland, ISBN 978-9914-733-97-6, 2022.

Wright, C. J., Hindley, N. P., Alexander, M. J., Barlow, M., Hoffmann, L., Mitchell, C. N., Prata, F., Bouillon, M., Carstens, J., Clerbaux, C., Osprey, S. M., Powell, N., Randall, C. E., and Yue, J.: Surface-to-space atmospheric waves from Hunga Tonga–Hunga Ha'apai eruption, Nature, 609, 741–746, https://doi.org/10.1038/s41586-022-05012-5, 2022.

https://doi.org/10.5194/egusphere-2026-3619
Preprint. Discussion started: 26 June 2026


Zhou, X., Dhomse, S. S., Feng, W., Mann, G., Heddell, S., Pumphrey, H., Kerridge, B. J., Latter, B., Siddans, R., Ventress, L., Querel, R., Smale, P., Asher, E., Hall, E. G., Bekki, S., and Chipperfield, M. P.: Antarctic Vortex Dehydration in 2023 as a Substantial Removal Pathway for Hunga Tonga-Hunga Ha'apai Water Vapor, Geophysical Research Letters, 51, e2023GL107 630, https://doi.org/10.1029/2023GL107630, 2024.

Zhou, X., Chen, Q., Feng, W., Heddell, S., Dhomse, S. S., Mann, G., Pumphrey, H. C., Millán, L., Santee, M. L., and Chipperfield, M. P.: Residence time of Hunga stratospheric water vapour perturbation quantified at 9 years, Communications Earth & Environment, https://doi.org/10.1038/s43247-026-03216-5, 2026.

Zhu, Y., Akiyoshi, H., Aquila, V., Asher, E., Bednarz, E. M., Bekki, S., Brühl, C., Butler, A. H., Case, P., Chabrillat, S., Chiodo, G., Clyne, M., Falletti, L., Colarco, P. R., Fleming, E., Jörimann, A., Kovilakam, M., Koren, G., Kuchar, A., Lebas, N., Liang, Q., Liu, C.-C., Mann, G., Manyin, M., Marchand, M., Morgenstern, O., Newman, P., Oman, L. D., Østerstrøm, F. F., Peng, Y., Plummer, D., Quaglia, I., Randel, W., Rémy, S., Sekiya, T., Steenrod, S., Sukhodolov, T., Tilmes, S., Tsigaridis, K., Ueyama, R., Visioni, D., Wang, X., Watanabe, S., Yamashita, Y., Yu, P., Yu, W., Zhang, J., and Zhuo, Z.: Hunga Tonga-Hunga Ha'apai Volcano Impact Model Observation Comparison (HTHH-MOC) Project: Experiment Protocol and Model Descriptions, https://doi.org/https://doi.org/10.5194/gmd-18-5487-2025, 2024.

Zi, Y., Long, Z., Sheng, J., Lu, G., Perrie, W., and Xiao, Z.: The Sudden Stratospheric Warming Events in the Antarctic in 2024, Geophysical Research Letters, 52, e2025GL115 257, https://doi.org/10.1029/2025GL115257, 2025.

Østerstrøm, F. F., Santee, M. L., et al.: Effects of the Hunga eruption on stratospheric ozone and related trace gases, in APARC, 2025: The Hunga Eruption Atmospheric Impacts Report [Yunqian Zhu, Graham Mann, Paul A. Newman, William Randel (Eds.)]. APARC Report No. 11, WCRP Report No. 10/2025, https://doi.org/10.34734/FZJ-2025-05242, 2025.